



Absence of the KhpA and KhpB (JAG/EloR) RNA-binding proteins suppresses the requirement for PBP2b by overproduction of FtsA in *Streptococcus pneumoniae* D39

Jiaqi J. Zheng,¹ Amilcar J. Perez,¹
Ho-Ching Tiffany Tsui,^{1*} Orietta Massidda ² and
Malcolm E. Winkler ^{1*}

¹Department of Biology, Indiana University
Bloomington (IUB), Bloomington, IN 47405, USA.

²Dipartimento di Scienze Chirurgiche, Università di
Cagliari, 09100 Cagliari, Italy.

Summary

Suppressor mutations were isolated that obviate the requirement for essential PBP2b in peripheral elongation of peptidoglycan from the midcells of dividing *Streptococcus pneumoniae* D39 background cells. One suppressor was in a gene encoding a single KH-domain protein (KhpA). $\Delta khpA$ suppresses deletions in most, but not all (*mltG*), genes involved in peripheral PG synthesis and in the *gpsB* regulatory gene. $\Delta khpA$ mutations reduce growth rate, decrease cell size, minimally affect shape and induce expression of the WalRK cell-wall stress regulon. Reciprocal co-immunoprecipitations show that KhpA forms a complex in cells with another KH-domain protein (KhpB/JAG/EloR). $\Delta khpA$ and $\Delta khpB$ mutants phenocopy each other exactly, consistent with a direct interaction. RNA-immunoprecipitation showed that KhpA/KhpB bind an overlapping set of RNAs in cells. Phosphorylation of KhpB reported previously does not affect KhpB function in the D39 progenitor background. A chromosome duplication implicated FtsA overproduction in $\Delta pbp2b$ suppression. We show that cellular FtsA concentration is negatively regulated by KhpA/B at the post-transcriptional level and that FtsA overproduction is necessary and sufficient for suppression of $\Delta pbp2b$. However, increased FtsA only partially accounts for the phenotypes of $\Delta khpA$ mutants. Together, these results suggest that

multimeric KhpA/B may function as a pleiotropic RNA chaperone controlling pneumococcal cell division.

Introduction

Streptococcus pneumoniae (pneumococcus; *Spn*) is both a commensal bacterium of the human nasopharynx and a serious opportunistic bacterial pathogen that kills millions of people annually worldwide, despite progress in the distribution of conjugated vaccines (Henriques-Normark and Tuomanen, 2013; Vernatter and Pirofski, 2013; Ferreira and Gordon, 2015; Gratz *et al.*, 2015; Oliver and Swords, 2015; Siegel and Weiser, 2015; Iovino *et al.*, 2016). Of utmost concern, *S. pneumoniae* has emerged as a ‘superbug’ pathogen, whose antibiotic resistance presents an imminent threat to human health (CDC, 2013; WHO, 2017). *S. pneumoniae* is a low-GC, Gram-positive ovoid-shaped (ovococcus) bacterium (see Supporting Information Fig. S1A). The ovoid shape, size and chaining of *S. pneumoniae* cells are determined by the peptidoglycan (PG) cell wall, which is a mesh-like macromolecule around the cytoplasmic membrane (Typas *et al.*, 2012; Turner *et al.*, 2014; Egan *et al.*, 2015; Egan *et al.*, 2017). In Gram-positive pathogens, like *S. pneumoniae* (Supporting Information Fig. S1A), PG acts as a scaffold for attachment of other surface macromolecules involved in virulence and host interactions, such as wall teichoic acids, sortase-attached proteins and capsule (Massidda *et al.*, 2013; Brown *et al.*, 2015). Steps in surface-exposed PG biosynthesis are targets for many of the antibiotics to which resistance has developed in a range of bacterial pathogens (Hakenbeck *et al.*, 2012; CDC, 2013; Walsh and Wenciewicz, 2016).

In ovococci like *S. pneumoniae*, the equator of newly divided cells becomes the midcell septum from which FtsZ-ring mediated division and peptidoglycan (PG) elongation occur (Supporting Information Fig. S1A) (Zapun *et al.*, 2008; Massidda *et al.*, 2013; Pinho *et al.*, 2013; Fleurie *et al.*, 2014; Tsui *et al.*, 2014; Jacq *et al.*,

Accepted 20 September, 2017. *For correspondence. E-mail winklerm@indiana.edu; Tel. 812-856-1318; Fax 812-855-6705. E-mail ttttsui@indiana.edu; Tel. 812-856-1781; Fax 812-855-6705.

2015). The septal PG synthesis machine utilizes class B PBP2x (designated here as 'bPBP2x' to indicate class) and other proteins to synthesize the PG wall between daughter cells, whereas the peripheral (sidewall-like) PG synthesis machine uses class B PBP2b (designated here as 'bPBP2b') and other proteins to push PG outward from the midcell division ring to elongate cells (Berg *et al.*, 2013; Massidda *et al.*, 2013; Morlot *et al.*, 2013; Tsui *et al.*, 2014). In mid-to-late stages of cell division, bPBP2x localizes separately from bPBP2b and other proteins to complete synthesis of the septal ring (Tsui *et al.*, 2014; Rued *et al.*, 2017). Balance between septal and peripheral PG synthesis to produce ovoid-shaped cells is mediated by the GpsB switching protein in complexes with the StkP Ser/Thr protein kinase and other division proteins (Land *et al.*, 2013; Fleurie *et al.*, 2014; Rued *et al.*, 2017). Concurrent with PG synthesis, PG hydrolases remodel the PG during closure of the septal ring and separation of daughter cells (Vollmer *et al.*, 2008; Barendt *et al.*, 2011; Sham *et al.*, 2012; Boersma *et al.*, 2015; Pazos *et al.*, 2017).

In previous studies, we isolated suppressor mutations that allowed growth of knock-out mutants in essential PG synthesis genes, such as Δ *gpsB* and Δ *pbp2b* (Tsui *et al.*, 2016; Rued *et al.*, 2017). Mutations that inactivate the PhpP Ser/Thr protein phosphatase suppressed Δ *gpsB* and led to further characterization of the effects of GpsB on protein phosphorylation catalyzed by the StkP kinase (Fleurie *et al.*, 2014; Rued *et al.*, 2017). Suppressor analysis of Δ *pbp2b* led to the discovery of a new, essential protein (MltG), that likely functions as an endo-lytic transglycosylase in peripheral PG synthesis (Supporting Information Fig. S1B) (Tsui *et al.*, 2016). A very recent paper independently confirmed that *mltG* mutations suppress Δ *pbp2b* (Stamsås *et al.*, 2017). A current model for the composition of the peripheral PG synthesis machine (Supporting Information Fig. S1B) (Massidda *et al.*, 2013; Philippe *et al.*, 2014) includes: bPBP2b (transpeptidase (TP) that catalyzes mucopeptide crosslinks) (Berg *et al.*, 2013; Tsui *et al.*, 2014); class A PBP1a (designated here as 'aPBP1a' that acts as a transglycosylase (TG) to catalyze glycan chain formation and as a TP) (Land and Winkler, 2011; Fenton *et al.*, 2016; Tsui *et al.*, 2016; Straume *et al.*, 2017); MreC, MreD, RodZ and CozE (regulators of aPBP1a and other proteins) (Land and Winkler, 2011; Philippe *et al.*, 2014; Fenton *et al.*, 2016; Tsui *et al.*, 2016; Straume *et al.*, 2017); RodA (likely regulator of bPBP2b (Tsui *et al.*, 2016) with TG (Meeske *et al.*, 2016) and/or Lipid II flippase activity (Ruiz, 2015; Leclercq *et al.*, 2017); and MltG (likely endo-lytic transglycosylase that may release glycan chains for crosslinking) (Tsui *et al.*, 2016; Stamsås *et al.*, 2017). In the genetic background of the virulent serotype 2 D39 progenitor strain, these

proteins are singly essential, except for aPBP1a, whose absence results in significantly smaller ovoid-shaped cells with an increased aspect ratio compared to wild-type cells (Land and Winkler, 2011; Tsui *et al.*, 2016).

Besides *mltG* mutations, we identified mutations or duplications in other genes that suppresses the requirement for essential bPBP2b (Tsui *et al.*, 2016). One of these suppressor mutations is a frameshift mutation in a small (79 amino acid) ORF that encodes a single-KH domain protein, which we designate 'KhpA' (Fig. 1A). KH domains are well-characterized RNA-binding structures that contain a conserved GXXG motif between two alpha helices (Valverde *et al.*, 2008; Nicastro *et al.*, 2015). This conserved GXXG loop interacts with RNA backbone residues (Valverde *et al.*, 2008; Nicastro *et al.*, 2015). All KH domains form three-stranded β -sheets packed against three α -helices, and most prokaryotic KH domains exhibit the type II $\alpha\beta\alpha\alpha\beta$ topology (Valverde *et al.*, 2008; Nicastro *et al.*, 2015). Usually, KH domains are found with other domains in proteins that function by binding to RNA, such as transcription factors (e.g., NusA), ribosomal proteins or post-transcriptional RNA modifiers. However, single-KH domain RNA-binding proteins are found in important bacterial pathogens, including *Streptococcus* and *Enterococcus* species, *Bacillus anthracis*, *Chlamydia trachomatis* and *Mycobacterium tuberculosis* (Supporting Information Fig. S2).

In this article, we show that the absence of KhpA drastically reduces cell size, but largely maintains cell shape. Co-immunoprecipitation (Co-IP) experiments show that KhpA forms a complex with another RNA binding protein that we designate as 'KhpB', which was previously identified by Branny, Doubravová and coworkers as a JAG-domain protein phosphorylated by the StkP Ser/Thr protein kinase in *Spn* (Ulrych *et al.*, 2016). In new work, Håvarstein and coworkers reported independently that the absence of KhpB, which they called 'EloR', suppresses the requirement for bPBP2b in *Spn* (Stamsås *et al.*, 2017). Physiological experiments reported here show that the absence of the KhpA/B RNA binding protein increases the cellular concentration of the FtsA division protein through a post-transcriptional mechanism, and this increase in FtsA amount is necessary and sufficient for suppression of Δ *pbp2b*. Moreover, patterns of suppression suggest that KhpA/B regulates expression of proteins other than FtsA, and the absence of the KhpA/B RNA binding proteins induces PG stress, resulting in a strong increase in expression of the WalRK TCS regulon. Together, these results suggest that KhpA/B is a general RNA binding protein that may act as a chaperone/regulator analogous to Hfq in Gram-negative bacteria.

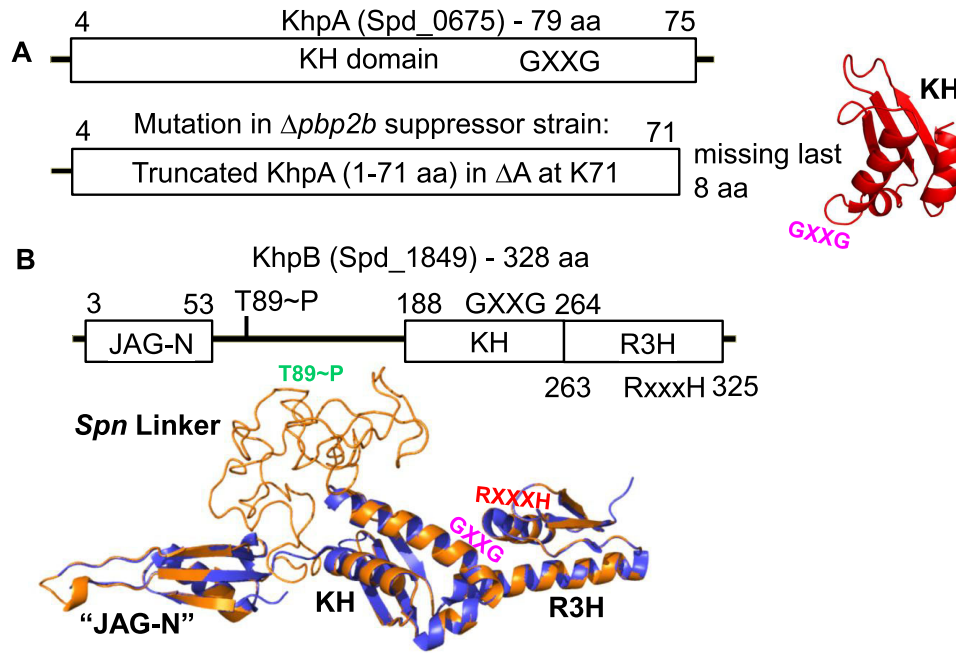


Fig. 1. Domain and modeled structures of KhpA (Spd_0675) and KhpB (Spd_1849) (not drawn to scale).

A. KhpA contains only one KH ('K Homology') RNA-binding domain (amino acids (aa) 4–75). Truncated KhpA in the original D39 Δcps $\Delta pbp2b$ *sup1* suppressor strain (Supporting Information Table S2) is indicated. The structure of KhpA was modeled as described in Experimental procedures. The location of the GXXG motif in KhpA is indicated.

B. KhpB contains a Jag-N domain of unknown function, KH and R3H ('RXXXH') RNA-binding domains. KhpB is phosphorylated by StkP at T89 and one other residue (Ulrych *et al.*, 2016; Stamsås *et al.*, 2017). KhpB structure (tan) was modeled on the known structure of the KhpB homologue of *Clostridium symbiosum* (purple), which lacks a large linker region between its JAG-N and KH domains. The large linker region of *Spn* KhpB, which contains phosphorylated T89, lacks predicted domains, and its structure is unknown. The locations of the GXXG (KH) and RXXXH (R3H) motifs and T89~P (*Spn* Linker) are marked.

Results

Mutations in *khpA* suppress $\Delta pbp2b$

pbp2b is essential in *S. pneumoniae* strains (Berg *et al.*, 2013; Tsui *et al.*, 2014; 2016; Stamsås *et al.*, 2017). Previously, we reported the isolation of five independent $\Delta pbp2b$ suppressor mutations in an unencapsulated (Δcps) derivative of strain D39 (Tsui *et al.*, 2016). Strain D39 is the progenitor of numerous laboratory strains, which have accumulated additional mutations that suppress or alter cell division phenotypes (Lanie *et al.*, 2007; Land and Winkler, 2011; Rued *et al.*, 2017). Four of the $\Delta pbp2b$ suppressors contained mutations in the *mltG* gene (Tsui *et al.*, 2016). The fifth suppressor strain contained wild-type *mltG*⁺, and mutations in three different genes: *spd_0268*(S189C), *spd_0675*(frameshift) and *crcB1*(S72L) (Supporting Information Table S2). We reconstructed these mutations separately in the wild-type D39 background and found that the frameshift mutation in *spd_0675* (ΔA at K71) suppressed $\Delta pbp2b$ (Table 1, line 8). In addition, we constructed a Δspd_0675 markerless mutation that suppressed $\Delta pbp2b$ (Table 1, line 9).

spd_0675 encodes a small protein of 79 amino acids with a molecular mass of 9 kDa. Spd_0675 consists of

only a single KH domain (Fig. 1A) (Valverde *et al.*, 2008; Nicastro *et al.*, 2015) and was accordingly designated as 'KhpA' (KH-domain protein A). The *khpA*(ΔA K71) frameshift mutation in the $\Delta pbp2b$ suppressor mutant truncated the last 8 amino acids of KhpA, including 4 amino acids of the KH domain, but left the GXXG RNA-interaction loop motif intact (Fig. 1A) (Valverde *et al.*, 2008; Nicastro *et al.*, 2015). Modeling described in Experimental procedures predicts that the structure of KhpA has the type II $\alpha\beta\beta\alpha\alpha\beta$ topology, characteristic of prokaryotic KH domains (Fig. 1A) (Valverde *et al.*, 2008; Nicastro *et al.*, 2015). KhpA is widely conserved in Gram-positive species, including several important low- and high-GC Gram-positive pathogens, including various *Streptococcus* species and *B. anthracis*, and *M. tuberculosis* respectively (Supporting Information Fig. S2). The pneumococcal KhpA homologue is closely related to KhpA of *C. trachomatis*. Single-KH domain proteins like KhpA have been annotated in numerous bacterial genomes, but their functions are generally unknown. Because *khpA* mutations suppress the requirement for bPBP2b in peripheral PG synthesis (Table 1), we hypothesized that KhpA regulates PG synthesis in *S. pneumoniae*.

Table 1. Suppression of mutations deficient in peripheral PG synthesis by $\Delta khpA$ or $\Delta khpB$ mutations or by ectopic overexpression of *ftsA*.^a

| Amplicon | Recipient strains | Number of colonies 20 h after transformation ^b |
|---|---|---|
| 1. $\Delta pbp2b \langle \rangle aad9$ | WT (IU1824) | 0 |
| 2. $\Delta mreCD \langle \rangle aad9$ | | 0 |
| 3. $\Delta rodZ \langle \rangle aad9$ | | 0 |
| 4. $\Delta rodA::P_c-erm$ | | 0 |
| 5. $\Delta mltG::P_c-erm$ | | 0 |
| 6. $\Delta coxE::P_c-erm$ | | >500 tiny colonies ^c |
| 7. $\Delta gpsB \langle \rangle aad9$ | | 0 |
| 8. $\Delta pbp2b \langle \rangle aad9$ | <i>khpA</i> (ΔA at K71) (IU7942) | >500 |
| 9. $\Delta pbp2b \langle \rangle aad9$ | $\Delta khpA$ (IU9036) | >500 |
| 10. $\Delta mreCD \langle \rangle aad9$ | | >500 |
| 11. $\Delta rodZ \langle \rangle aad9$ | | >500 |
| 12. $\Delta rodA::P_c-erm$ | | >500 |
| 13. $\Delta mltG::P_c-erm$ | | 0 ^d |
| 14. $\Delta coxE::P_c-erm$ | | >500 tiny colonies ^c |
| 15. $\Delta gpsB \langle \rangle aad9$ | | >500 |
| 16. $\Delta pbp2b \langle \rangle aad9$ | $\Delta khpB$ (IU10592) | >500 |
| 17. $\Delta mreCD \langle \rangle aad9$ | | >500 |
| 18. $\Delta rodZ \langle \rangle aad9$ | | >500 |
| 19. $\Delta rodA::P_c-erm$ | | >500 |
| 20. $\Delta mltG::P_c-erm$ | | 0 |
| 21. $\Delta gpsB \langle \rangle aad9$ | | >500 |
| 22. $\Delta pbp2b \langle \rangle aad9$ | <i>ftsA</i> ⁺ // <i>P</i> _{Zn} - <i>ftsZ</i> ⁺ (IU12286) | 0 |
| 23. $\Delta pbp2b \langle \rangle aad9$ | <i>ftsZ</i> ⁺ // <i>P</i> _{Zn} - <i>ftsZ</i> ⁺ + Zn ^e | ~100, tiny colonies |
| 24. $\Delta pbp2b \langle \rangle aad9$ | <i>ftsA</i> ⁺ // <i>P</i> _{Zn} - <i>ftsA</i> ⁺ (IU12310) | 0 |
| 25. $\Delta pbp2b \langle \rangle aad9$ | <i>ftsA</i> ⁺ // <i>P</i> _{Zn} - <i>ftsA</i> ⁺ + Zn ^e | >500 |
| 26. $\Delta mreCD \langle \rangle aad9$ | | >500 |
| 27. $\Delta rodZ \langle \rangle aad9$ | | 0 |
| 28. $\Delta rodA::P_c-erm$ | | >500 |
| 29. $\Delta gpsB \langle \rangle aad9$ | | 0 |

a. Recipient strains and amplicons were obtained as described in Supporting Information Table S1. Transformations with indicated amplicons were performed as described in Experimental procedures. Each transformation experiment was performed three times independently with similar results.

b. Unless indicated, transformant colonies were normal sized and generally uniform, typical of the recipient strain. See text for details about the growth properties of $\Delta khpA$ and $\Delta khpB$ mutants.

c. Direct transformation of a $\Delta coxE::P_c-erm$ amplicon into IU1824, D39 and other D39-derived strains resulted in tiny colonies that grew slowly. $\Delta khpA$ or $\Delta khpB$ did not rescue the growth defect of the $\Delta coxE::P_c-erm$ transformants.

d. Control experiments were performed showing that the $\Delta mltG::P_c-erm$ amplicon did transform a $\Delta pbp1a$ mutant or a merodiploid strain expressing two copies of *mltG*⁺ (Tsui *et al.*, 2016).

e. 0.5 mM ZnCl₂ + 0.05 mM MnSO₄ were added to transformation mixes and in subsequent steps to induce expression of *ftsZ* or *ftsA* under control of the *P*_{Zn} zinc-inducible promoter in the ectopic *bgaA* site. Mn²⁺ of 0.05 mM was added to eliminate toxicity caused by addition of 0.5 mM Zn²⁺ (Jacobsen *et al.*, 2011; Martin *et al.*, 2017a; Martin *et al.*, 2017b). Transformants of the *ftsA*⁺//*P*_{Zn}-*ftsA*⁺ recipient from TSAII-BA + Zn plates re-streaked at normal densities on fresh plates containing +Zn, but did not re-streak on plates lacking +Zn. Given the relatively high frequency of transformation and normal growth, it is unlikely that these different transformants picked up additional suppressor mutations that are still dependent on +Zn and *FtsA* overexpression.

ΔkhpA mutations reduce growth rate, decrease cell size, minimally reduce aspect ratio and induce expression of the WalRK TCS cell-wall stress regulon

The markerless $\Delta khpA$ mutation removed the central 73 amino acids of *khpA*, leaving 4 and 2 amino acids from the N- and C-termini, respectively, fused in-frame (strain IU9036, Supporting Information Table S1). The $\Delta khpA$ mutant grew $\approx 53\%$ slower than the wild-type parent in BHI broth (Fig. 2A). Expression of wild-type *KhpA* from the ectopic *bgaA* site complemented growth of the $\Delta khpA$ mutant back to the wild-type level. $\Delta khpA$ mutant cells had shorter cell lengths (by $\approx 30\%$) and widths (by $\approx 23\%$) compared to wild-type cells; however, overall cell shape was largely maintained with a reduction in aspect ratio of the $\Delta khpA$ mutant of only $\approx 10\%$ (Fig. 2B and D). Notably, the relative volume of $\Delta khpA$ cells was substantially reduced by $\approx 50\%$ compared to parent cells (Fig. 2B and D). Ectopic expression of *khpA*⁺ complemented the dimension defects of the $\Delta khpA$ mutant back almost (within 10%) to wild-type sizes. Similar growth and cell morphology defects were observed for $\Delta khpA$ mutants of the encapsulated, virulent serotype 2 D39 and serotype 4 TIGR4 strains (Supporting Information Fig. S3).

Proteins with KH domains generally bind RNA and function as regulators. Therefore, we performed an mRNA-Seq analysis of the $\Delta khpA$ mutant growing exponentially in BHI broth (Supporting Information Table S3). Unexpectedly, the relative amounts of only 19 mRNA transcripts changed significantly (threshold 1.8-fold) in the $\Delta khpA$ mutant compared to the parent, despite the slower growth and smaller cell size of the $\Delta khpA$ mutant (Fig. 2A, B and D). In particular, relative transcript amounts were greatly induced for genes controlled by the WalRK two-component system (TCS), which maintains PG homeostasis and responds to PG cell wall stress in *Spn* and other low-GC Gram-positive bacteria (Supporting Information Table S3, top) (Ng *et al.*, 2005; Dubrac *et al.*, 2008; Gutu *et al.*, 2010; Fritz and Mascher, 2014; Tsui *et al.*, 2016). Beside induction of the WalRK regulon, small changes (1.8- to 3.2-fold) in relative transcript amounts were detected for several other stress-responsive genes, possibly due to the impaired growth of the $\Delta khpA$ mutant compared to the parent (Supporting Information Table S3, middle).

We confirmed induction of relative transcript amounts of two WalRK TCS regulon genes (*spd_1874* and *spd_0104*) in the $\Delta khpA$ mutant by qRT-PCR (Fig. 2C). Both genes, which encode extracellular proteins containing LysM domains (Ng *et al.*, 2005; Barendt *et al.*, 2011), were strongly induced in the $\Delta khpA$ mutant, and the induction was complemented back to the wild-type level by ectopic expression of *khpA*⁺. Previously, we reported induction of the WalRK regulon in mutants deficient in peripheral PG synthesis, including $\Delta pbp1a$,

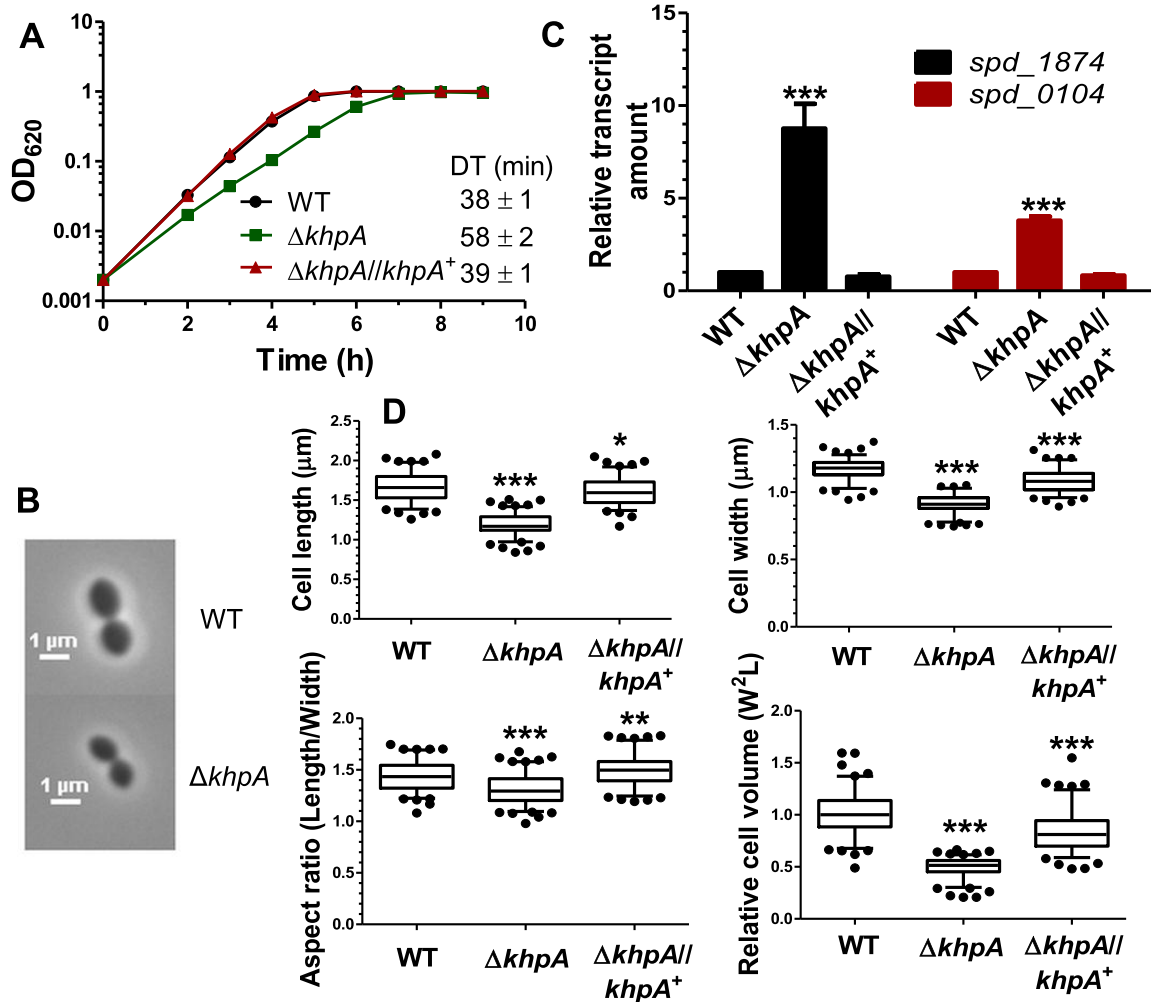


Fig. 2. $\Delta khpA$ mutations reduce growth rate, decrease cell size, minimally reduce aspect ratio and induce expression of the WalRK TCS stress regulon. Wide-type (WT) (IU1824), $\Delta khpA$ (IU9036) and $\Delta khpA//khpA^+$ (IU9621; complementation) strains were compared. A. Growth curves in BHI broth. Doubling times (DT) were calculated from three independent growth curves for cells growing exponentially ($OD_{620} = 0.03-0.3$).

B. Representative phase-contrast images of cells in early exponential phase. Scale bar = 1 μm .

C. Relative transcript amounts of *spd_1874* and *spd_0104* of the WalRK regulon in $\Delta khpA$ and $\Delta khpA//khpA^+$ mutants compared to WT, determined by qRT-PCR as described in Experimental procedures. Averages \pm SE are shown from three independent experiments.

D. Box-and-whisker plots (whiskers, 5 and 95 percentile) of cell length, width, aspect ratio (length/width) and relative cell volume of WT, $\Delta khpA$ and $\Delta khpA//khpA^+$ cells; >100 cells from exponential cultures were measured for each strain in two independent experiments. For C and D, *P* values were obtained relative to WT by one-way ANOVA analysis (GraphPad Prism). **P* < 0.05, ***P* < 0.01 and ****P* < 0.001.

$\Delta pbp1b$ or *mltG*(Y488D) (Tsui *et al.*, 2016). Taken together, the suppression of a $\Delta pbp2b$ mutation, decrease in growth rate, smaller cell size and induction of the WalRK regulon by $\Delta khpA$ support the hypothesis that the KhpA protein plays a fundamental role in PG homeostasis and regulating peripheral PG synthesis.

ΔkhpA suppresses ΔmreCD, ΔrodZ, ΔrodA and ΔgpsB, but not ΔmltG and ΔcozE

Previously, we showed that the *mltG*(Y488D) mutation, which likely reduces MltG enzymatic activity, suppressed $\Delta pbp2b$ and the requirement for all other essential

genes involved in peripheral PG synthesis, including $\Delta mreCD$, $\Delta rodZ$ and $\Delta rodA$ (Supporting Information Fig. S1B) (Tsui *et al.*, 2016). Since $\Delta khpA$ suppressed $\Delta pbp2b$ (Table 1, row 9), we tested whether $\Delta khpA$ would suppress mutations in essential genes involved in peripheral PG synthesis. $\Delta khpA$ suppressed $\Delta mreCD$, $\Delta rodZ$ and $\Delta rodA$ mutations (Table 1, lines 10–12). However, $\Delta khpA$ did not suppress $\Delta mltG$, nor did it improve the severely inhibited growth of a $\Delta cozE$ mutant under these conditions (Table 1, lines 13–14). Consistent with lack of suppression of $\Delta mltG$ by $\Delta khpA$, $\Delta khpA$ *mltG*(Y488D) double mutants grew much slower than $\Delta khpA$ or *mltG*(Y488D) single mutants (Supporting

Information Fig. S4). $\Delta pbp2b \Delta khpA$, $\Delta mreCD \Delta khpA$, $\Delta rodZ \Delta khpA$ and $\Delta rodA \Delta khpA$ double mutants had slower growth rates and reduced cell sizes similar to those of the $\Delta khpA$ mutant (Supporting Information Fig. S5), consistent with the same mechanism of peripheral PG synthesis bypass. Unexpectedly, $\Delta khpA$ mutants also partly suppressed the requirement for the GpsB switching protein (Table 1, row 15). In contrast to the double mutants described above, the $\Delta gpsB \Delta khpA$ double mutant grew considerably slower than the $\Delta khpA$ mutant and formed large, elongated cells, characteristic of GpsB depletion (Supporting Information Fig. S5B). We conclude that the absence of KhpA bypasses some, but not all of the proteins required for PG synthesis and that KhpA may regulate peripheral PG synthesis by a different pathway than GpsB function.

KhpA forms a complex with KH/R3H-domain protein KhpB (JAG/EloR) in S. pneumoniae cells

A single-KH domain protein like KhpA would recognize only about 4 nucleotides; therefore, KH domains are typically in multimeric proteins that contain additional domains (Valverde *et al.*, 2008; Nicastro *et al.*, 2015). Consequently, we hypothesized that KhpA may be in a complex with another RNA binding protein that would provide RNA binding strength and possibly specificity. To test this idea, we constructed a strain producing C-terminal, epitope-tagged KhpA-L-FLAG³ from its normal chromosomal locus (IU9602, Supporting Information Table S1). This strain, which does not exhibit any phenotypic defects of *khpA* mutants (Fig. 2, Supporting Information Figs S5 and S6), was crosslinked with formaldehyde, and KhpA-L-FLAG³ was used as bait in co-immunoprecipitation experiments (co-IP) (see Experimental procedures) (Rued *et al.*, 2017). After heating to reverse crosslinks, a single prominent band not seen in the control was visible on silver stained SDS-PAGE gels (Fig. 3, Lane 1). This protein was identified by mass spectrometry (MS) as Spd_1849, which is another putative RNA binding protein containing KH and R3H domains that we designated as 'KhpB' (KH-domain protein B; Fig. 1B). To confirm complex formation, the reciprocal co-IP experiment with crosslinking was performed in a strain expressing functional KhpB-L-FLAG³ from its native site, which is distant from *khpA* (see *spd* gene tags, Fig. 1). A single band not present in the control was detected and confirmed to be KhpA by MS (Fig. 3, lane 3).

Spn KhpB is a protein of 328 amino acids containing a misnamed amino-terminal 'JAG-N' domain of unknown function, a long linker region and the two tandem RNA binding domains (KH and R3H) (Fig. 1B). KhpB shows

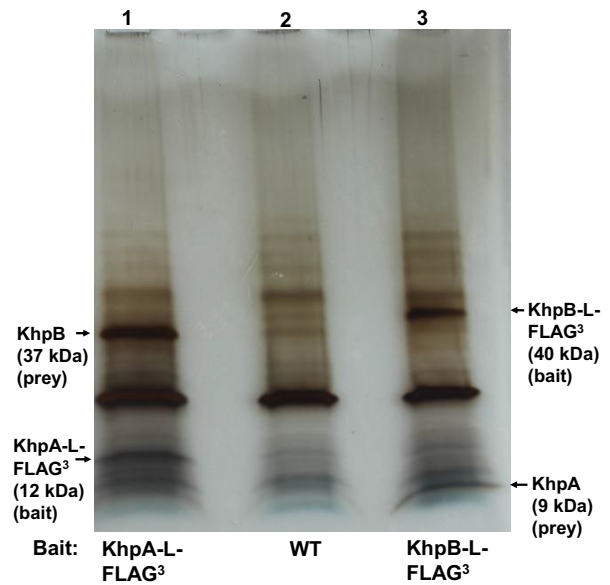


Fig. 3. KhpA forms a complex with RNA binding protein KhpB in cells.

Silver-stained SDS-PAGE gel from co-IP experiments, performed using KhpA-L-FLAG³ (IU9602, lane 1), WT (IU1945, lane 2 non-flagged control) or KhpB-L-FLAG³ (IU10664, lane 3) as bait (see Experimental procedures). Prey bands from lanes 1 and 3 were identified by MS as KhpB and KhpA respectively. The experiment was performed independently twice. Indicated calculated molecular masses of bands are consistent with a standard ladder that is not shown.

a similarly wide distribution among different bacterial species as KhpA (Supporting Information Fig. S2). Recently, KhpB (called 'JAG') was independently identified as a protein phosphorylated at T89 and at least one other residue, by the StkP protein kinase of *Spn* (Ulrych *et al.*, 2016). Very recently, $\Delta khpB$ (called ' $\Delta eloR$ ') mutations were independently discovered as suppressors of $\Delta pbp2b$ in laboratory strain R6 (Stamsås *et al.*, 2017). We conclude that KhpA and KhpB are in a complex together in *Spn* cells, and given the strength and singularity of the reciprocal co-IPs (Fig. 3), it is likely that KhpA and KhpB interact directly with each other.

$\Delta khpB$ mutants phenocopy $\Delta khpA$ mutants exactly for growth and morphology

If KhpA and KhpB directly interact in an obligatory complex, then we would expect $\Delta khpA$, $\Delta khpB$ and $\Delta khpA \Delta khpB$ mutants to phenocopy each other. Previously, Branny, Doubravová and coworkers showed that $\Delta khpB$ mutants grow slightly slower and form smaller cells with a nearly unchanged aspect ratio compared to the parent in the Rx1 laboratory strain background (Ulrych *et al.*, 2016). This phenotype is similar to that of $\Delta khpA$ mutants (Fig. 2). We further showed that markerless

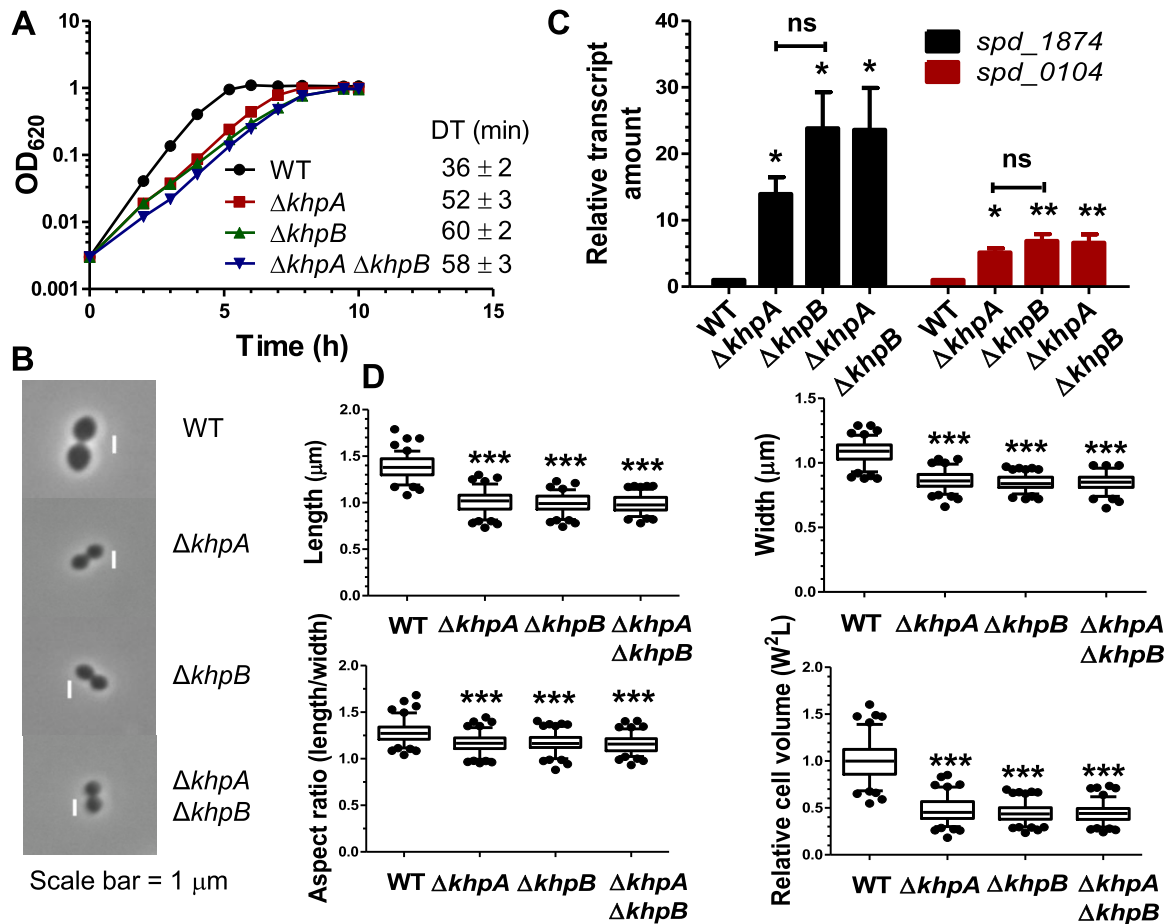


Fig. 4. $\Delta khpB$ mutants phenocopy $\Delta khpA$ mutants exactly. WT (IU1824), $\Delta khpA$ (IU9036), $\Delta khpB$ (IU10592) and $\Delta khpA \Delta khpB$ (IU10596) mutants were compared.

A. Growth curves in BHI broth. Doubling times (DT) were calculated from three independent growth curves for cells growing exponentially ($OD_{620} = 0.03\text{--}0.3$).

B. Representative phase-contrast images of cells in early exponential phase. Scale bar = 1 μm .

C. Relative transcript amounts of *spd_1874* and *spd_0104* of the WaiRK regulon in $\Delta khpA$, $\Delta khpB$ and $\Delta khpA \Delta khpB$ mutants compared to WT, determined by qRT-PCR as described in Experimental procedures. Averages \pm SE are shown from three independent experiments.

D. Box-and-whisker plots (whiskers, 5 and 95 percentile) of cell length, width, aspect ratio (length/width) and relative cell volume of WT, $\Delta khpA$, $\Delta khpB$ and $\Delta khpA \Delta khpB$ cells; >100 cells from exponential cultures were measured for each strain in two independent experiments. For C and D, *P* values were calculated as for Fig. 2. ns, not significantly different.

$\Delta khpA$, $\Delta khpB$ and $\Delta khpA \Delta khpB$ mutations led to similar slower growth, decreased cell lengths and widths, minimally reduced aspect ratios, significantly decreased relative cell volumes (\approx twofold) and induction of the WaiRK regulon (Fig. 4). $\Delta khpA \Delta khpB \Delta pbp2b$ triple mutants showed similar slower growth and smaller cell size as $\Delta khpA$ or $\Delta khpB$ single mutants or $\Delta khpA \Delta pbp2b$ double mutants compared to the wild-type strain (Supporting Information Figs S5 and S7). $\Delta khpB$ suppressed the same mutations in peripheral PG synthesis ($\Delta pbp2b$, $\Delta mreCD$, $\Delta rodZ$, $\Delta rodA$, but not $\Delta mltG$) and PG synthesis regulation ($\Delta gpsB$) as $\Delta khpA$ (Table 1, lines 9–15 and 16–21). Recently, $\Delta khpB$ ($\Delta eloF$) mutants were reported to suppress $\Delta pbp2b$ and $\Delta rodA$ in laboratory strain R6, where *mreCD* and *rodZ* are not essential (Straume *et al.*, 2017) and *pbp1a* is mutated (Lanie *et al.*, 2007; Land

and Winkler, 2011). After discovering the interaction between KhpA and KhpB (Fig. 3), we isolated additional spontaneous $\Delta pbp2b$ suppressors, which included three independent knock-out mutations in *khpB* (*sup7–9*, Supporting Information Table S2) and a null mutation in *khpA* (*sup10*, Supporting Information Table S2).

KhpA and KhpB co-localized at all stages of the cell cycle (Supporting Information Fig. S8). Unlike many *Spn* PG synthesis and division proteins (e.g., StkP, bPBP2b and FtsZ), KhpA and KhpB were diffuse in early divisional cells (Supporting Information Fig. S8B and S8C). There is some concentration of KhpA and KhpB at the midcells of dividing cells (Supporting Information Fig. S8B), as noted before in strain R6 (Stamsås *et al.*, 2017); however, there is still a diffuse distribution of the two proteins throughout cells (Supporting Information

Fig. S8B and S8C). The tendency of KhpA and KhpB to concentrate at midcells may reflect the interaction of KhpB as a substrate of the StkP protein kinase, which is confined tightly to midcells throughout division (Supporting Information Fig. S8B) (Beilharz *et al.*, 2012; Morlot *et al.*, 2013; Fleurie *et al.*, 2014; Tsui *et al.*, 2014). The degree of phosphorylation of MapZ/StkP and DivIVA mediated by the StkP kinase and PhpP phosphatase was reduced slightly by $\approx 20\text{--}40\%$ in $\Delta khpA$, $\Delta khpB$ and $\Delta khpA \Delta khpB$ mutants compared to the wild-type strain, perhaps with lower levels in $\Delta khpB$ mutants (Supporting Information Fig. S9). These small changes in phosphorylation of cell division proteins may partly be an indirect effect of the slower growth, decreased cell size and cell wall stress of these mutants (Figs 2 and 4). Taken together, the exact phenocopying by $\Delta khpA$, $\Delta khpB$ and $\Delta khpA \Delta khpB$ for growth and morphology provides strong physiological support that KhpA and KhpB interact and mediate the same regulatory pathways in pneumococcal cells.

To determine whether phosphorylation of KhpB at T89 by StkP kinase is important for KhpA/B function in the D39 genetic background, we constructed the *khpB*(T89A) phosphoablative mutation in the chromosome of strain IU1824 (IU12744; Supporting Information Table S1). *khpB*(T89A) did not cause the aberrant growth or morphological defects of $\Delta khpA/B$ mutants, indicating that T89~P phosphorylation of KhpB is not obligatory for its function under these culture conditions (Supporting Information Fig. S10). Likewise, *khpB*(T89D) (IU13881) or *khpB*(T89E) (IU13883) phosphomimetic mutants in the D39 background were readily constructed without any indication of suppressor accumulation in transformations (few colonies; colony heterogeneity), in contrast to what was reported for laboratory strain R6 (Stamsås *et al.*, 2017). *khpB*(T89D) or *khpB*(T89E) mutants also did not exhibit ostensible growth or cell morphology phenotypes (Supporting Information Fig. S10). Whole-genome sequencing of *khpB*(T89A), *khpB*(T89D) and *khpB*(T89E) mutants confirmed that no additional suppressor mutations are present (data not shown).

KhpA and KhpB interact with a similar set of RNAs in cells

Changing the KhpA(GRKG→GDDG) and KhpA(GRKG→ARKA) nucleic acid binding motif destabilized KhpA and resulted in a $\Delta khpA$ phenotype (Supporting Information Fig. S11). We performed RIP-Seq (RNA-immunoprecipitation) experiments without crosslinking using KhpA-L-FLAG³ or KhpB-L-FLAG³ as bait to demonstrate that KhpA and KhpB indeed bind to RNA in cells (see Experimental procedures) (Saadeh *et al.*, 2015). We

used the ratio of RNA reads obtained for each of the FLAG-tagged strains compared to the untagged wild-type strain as the criterion for RNA binding of RNA to KhpA or KhpB (Supporting Information Table S4). A separate RIP-qRT-PCR control experiment (Supporting Information Fig. S12) detected two transcripts enriched strongly by KhpA-L-FLAG³ and KhpB-L-FLAG³ in RIP-Seq (Supporting Information Table S4). In addition, a third putative RNA binding protein (Spd_1366-L-FLAG³) did not pull down the two transcripts pulled down by KhpA/B-L-FLAG³, indicating that the L-FLAG³ affinity tag was not affecting the RNAs recovered by RIP (Supporting Information Fig. S12). Several general conclusions emerged from the RIP-Seq experiments. With a fourfold enrichment as the cutoff (Saadeh *et al.*, 2015), KhpA or KhpB pulled down a remarkable overlapping set of ≈ 170 mRNA, tRNAs, intergenic RNAs and putative sRNAs (Fig. 5; Supporting Information Table S4). The strong overlap of the RNAs pulled down by KhpA or KhpB supports the idea that KhpA and KhpB interact in cells to form a complex that mediates different RNA interactions in multiple regulatory pathways. Hence, the KhpA and KhpB proteins and $\Delta khpA \Delta khpB$ mutants will be referred to as KhpA/B and $\Delta khpA/B$, respectively, in the rest of this article. Notably, many of the mRNAs pulled down by KhpA or KhpB correspond to small reading frames annotated as hypothetical proteins (Supporting Information Table S4). Three mRNAs corresponding to small proteins (Spd_0023 (80 aa); Spd_0963 (44 aa) and Spd_1159 (56 aa)) and two tRNAs (tRNA^{Thr} and tRNA^{P^{ro}}) were enriched by >10-fold by pull down with KhpA or KhpB (Supporting Information Table S4). The mRNAs of three cell division proteins (FtsA (twofold to threefold), SepF (\approx threefold), and Spd_0703 (\approx sevenfold) (Barendt *et al.*, 2011)) were preferentially pulled down by KhpA or KhpB (Supporting Information Table S4). An interaction of KhpA/B with a specific target near the 5'-UTR leader region of the *ftsA* transcript is described below.

FtsA overproduction is sufficient to suppress $\Delta pbp2b$

To understand suppression of $\Delta pbp2b$ by $\Delta khpA/B$, we selected for additional suppressor mutations and checked for *mltG*⁺, *khpA*⁺ and *khpB*⁺ alleles before whole-genome sequencing (*sup6*, Supporting Information Table S2). No mutations were detected in the *sup6* suppressor other than the expected Δcps and $\Delta pbp2b$ mutations. However, analysis of total genomic reads and junction points showed that *sup6* contains a large tandem chromosomal duplication of the region that contains the *ftsA-ftsZ* operon encoding the FtsA and FtsZ division proteins (Fig. 6; Experimental procedures). This

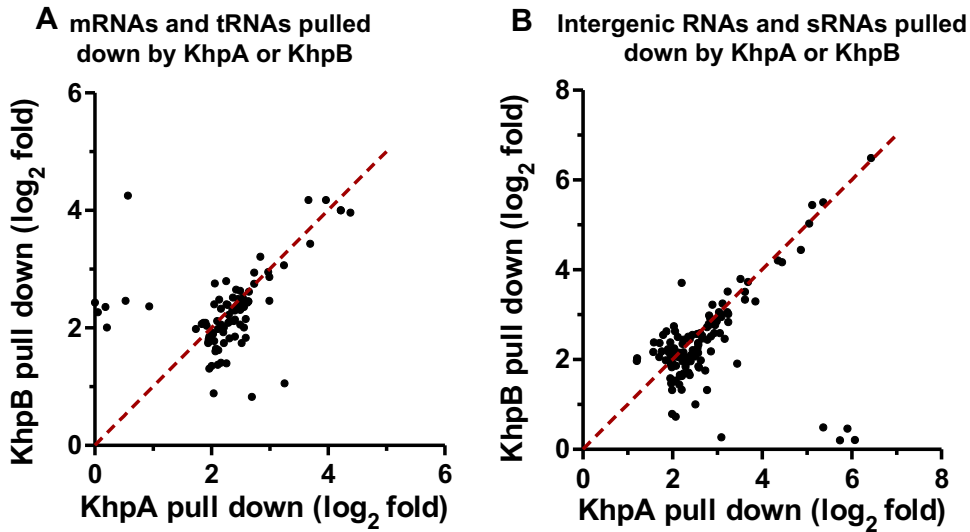


Fig. 5. KhpA and KhpB pull down overlapping sets of RNAs in RIP-Seq experiments. Scatter plots show the fold-changes (expressed as \log_2) for separate mRNAs and tRNAs (A; Supporting Information Table S4A) or intergenic RNAs and sRNAs (B; Supporting Information Table S4B) pulled down by KhpA-L-FLAG³ or KhpB-L-FLAG³ in RIP-Seq experiments, where fourfold enrichment was used as the cutoff.

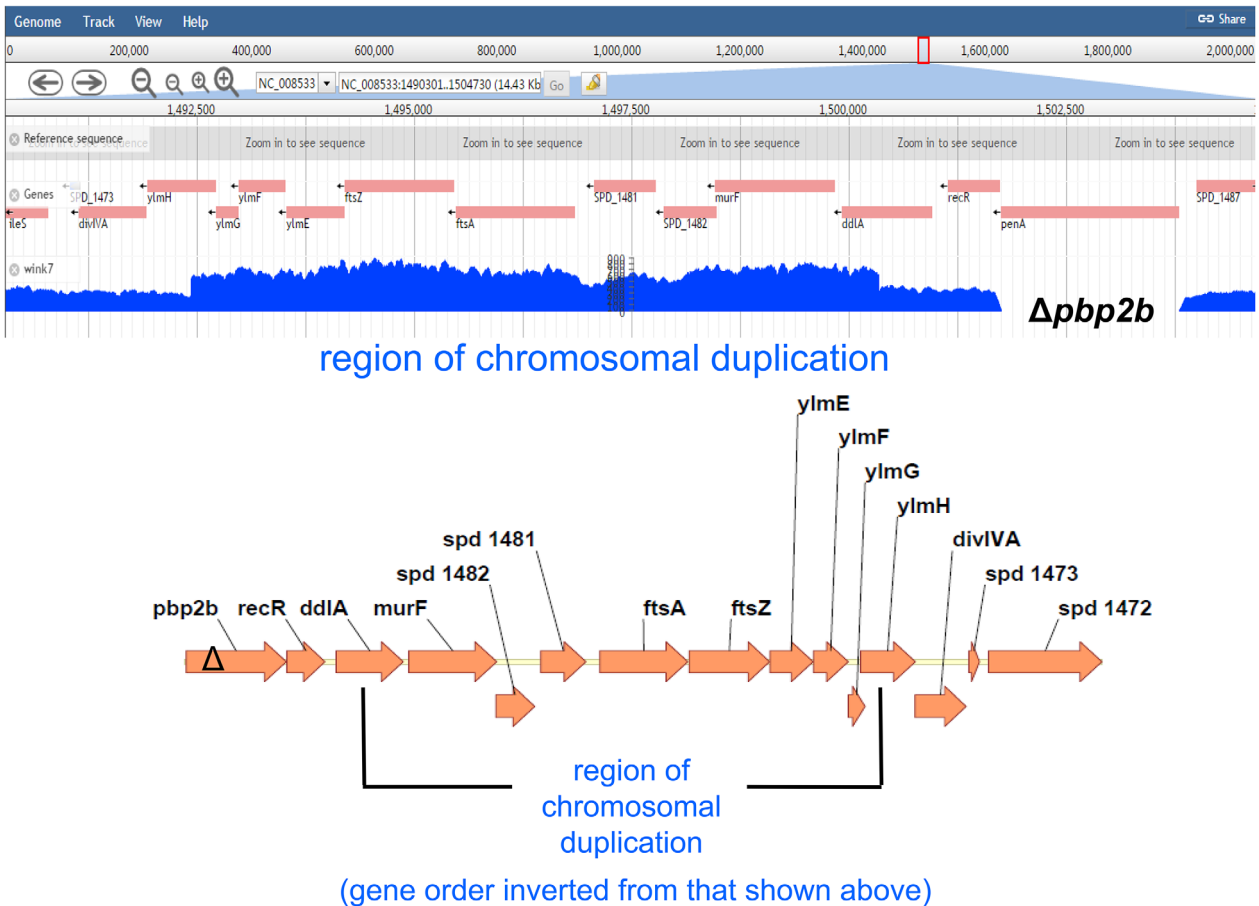


Fig. 6. The chromosomal region surrounding *ftsA-ftsZ* (*ddl-ylmH*) is tandemly duplicated in the Δ *pbp2b* *sup6* suppressor strain. Top, number of reads from Illumina NextSeq DNA sequencing showing that the *ddl-ylmH* region is duplicated in the Δ *pbp2b* *sup6* suppressor strain (Supporting Information Table S2). No other mutations were detected in this strain. The number of reads across the duplicated region is \approx twice that of the adjoining regions. As expected, there are no reads from *penA* (*pbp2b*), which is deleted in the Δ *pbp2b* suppressor strain. Reads spanning the junction between the 3' end of the repeat region to the 5' end of the repeat region were identified by bioinformatic analysis described in Experimental procedures, indicating that the repeat is a single tandem duplication that occurred in place without any other obvious re-arrangements taking place. Bottom, diagram of the annotated chromosomal region of the Ω (*ddl-ylmH*) region, including the *ftsA-ftsZ* operon, duplicated in the Δ *pbp2b* *sup6* suppressor.

Table 2. Transformation by a $\Delta pbp2b$ amplicon is dependent on overproduction of FtsA.^a

| Recipient strain | Number of colonies 20 h after transformation with a $\Delta pbp2b$ <>P _c -erm amplicon | Relative FtsA amount ^b (average ± SE) |
|--|---|--|
| 1. WT (IU1824) | 0 | ≡1.0 |
| 2. WT + Zn ^c | 0 | 0.9 ± 0.1 |
| 3. $\Delta khpA$ (IU9036) | >500 | 2.6 ± 1.0 |
| 4. $\Delta khpA$ + Zn ^c | >500 | 2.3 ± 0.1 |
| 5. $ftsA^+$ //P _{Zn} -ftsA ⁺ (IU12310) ^d | 0 | 1.1 ± 0.1 |
| 6. $ftsA^+$ //P _{Zn} -ftsA ⁺ + Zn ^{cd} | >500 | 2.6 ± 0.5 |
| 7. $\Delta ftsA$ //P _{Zn} -ftsA ⁺ + Zn (IU12901) ^{cd} | 0 | 1.0 ± 0.1 |
| 8. $\Delta khpA \Delta ftsA$ //P _{Zn} -ftsA ⁺ + Zn (IU12959) ^{cd} | 0 | 1.2 ± 0.2 |
| 9. $\Delta ftsA$ //P _{ftsA} -ftsA ⁺ (IU13201) ^e | 0 | 0.6 ± 0.1 |
| 10. $\Delta khpA \Delta ftsA$ //P _{ftsA} -ftsA ⁺ (IU13204) ^e | >500 | 2.3 ± 0.2 |
| 11. $ftsA(\Delta UTR)$ (IU13641) | 0 | 0.5 ± 0.1 |
| 12. $\Delta khpA ftsA(\Delta UTR)$ (IU13672) | 0 | 0.6 ± 0.1 |

a. Recipient strains and amplicons were obtained as described in Supporting Information Table S1. Transformations were performed as described in Experimental procedures. Each transformation experiment was performed three times independently with similar results.

b. FtsA amounts relative to WT were determined in cultures growing exponentially in BHI broth by quantitative Western blotting in the linear range of detection as described in Experimental procedures. Averages (± SE) are listed for three independent experiments, separate from other experiments in this article, except for lines 11–12, which are from Figure 7.

c. 0.5 mM ZnCl₂ + 0.05 mM MnSO₄ were added to induce expression of *ftsA* under control of the P_{Zn} zinc-inducible promoter in the ectopic *bgaA* site. Mn²⁺ of 0.05 mM was added to eliminate toxicity caused by addition of 0.5 mM Zn²⁺ (Jacobsen *et al.*, 2011; Martin *et al.*, 2017a; Martin *et al.*, 2017b).

d. Ectopic *bgaA*:: P_{Zn}-ftsA⁺ has the Zn²⁺-inducible P_{czcD} promoter (Mu *et al.*, 2013) fused to 22 bp from the *czcD* 5'-UTR leader, which is fused to the 24 bp of the *ftsA* 5'-UTR containing the RBS upstream of the *ftsA* start codon and reading frame (see Fig. 9A). *bgaA*:: P_{Zn}-ftsA⁺ does not produce most of the 74 nt *ftsA* 5'-UTR (ΔUTR) in its transcript.

e. Ectopic *bgaA*:: P_{ftsA}-ftsA⁺ contains the entire 218 bp intercistronic region between *spd_1481* and the *ftsA*⁺ gene (see Fig. 6, bottom). P_{ftsA}-ftsA⁺ produces the entire 74 nt *ftsA* 5'-UTR (UTR⁺) in its transcript (Fig. 9A).

duplication in *ftsA* resulted in an \approx threefold increase in FtsA cellular concentration (Supporting Information Fig. S13). FtsZ overproduction was previously shown to suppress $\Delta pbp2b$ mutations in *E. coli* that lack bPBP2 required for PG side-wall elongation (Vinella *et al.*, 1993; Bendezu and de Boer, 2008). We overproduced FtsZ by \approx 1.9-fold from a Zn²⁺-inducible promoter in an ectopic site (Supporting Information Fig. S14). Overproduction of FtsZ poorly suppressed $\Delta pbp2b$, resulting in tiny colonies that acquired fast-growing suppressors on re-streaking (Table 1, lines 22–23) [see (Tsui *et al.*, 2016)]. In contrast, overproduction of FtsA (\approx 2.6-fold) from an ectopic site substantially suppressed $\Delta pbp2b$ and allowed colony formation and growth in BHI broth (Table 1, lines 24–25; Table 2, lines 5–6; Fig. 7A and B; Supporting Information Fig. S15). A control experiment showed that ectopic overexpression of *ftsA* did not change the relative cellular amount of FtsZ (Supporting Information Fig. S15). Overproduction of FtsA resulted in slightly spherical, smaller cells than wild-type (Fig. 7C(2), Supporting Information Figs S16A and S16B), as reported previously (Mura *et al.*, 2017). FtsA overproduction did not restore wild-type morphology to $\Delta pbp2b$ cells and resulted in chains of slightly irregularly shaped, often spherical cells (Fig. 7C(4)). Depletion of excess FtsA in a $ftsA^+ \Delta pbp2b$ //P_{Zn}-ftsA⁺ mutant resulted in chains of enlarged spherical cells (Fig. 7C(4)), similar to those caused by bPBP2b depletion (Fig. 7C(3)). We conclude that \approx threefold overproduction of FtsA alone,

but not FtsZ, is sufficient to restore $\Delta pbp2b$ growth, without restoring wild-type cell morphology.

Cellular FtsA concentration is negatively regulated by KhpA/B at the post-transcriptional level

We tested whether the relative cellular amount of FtsA is increased in $\Delta khpA/B$ mutants. Quantitative Western blotting showed that cellular FtsA concentration is induced by \approx threefold in the $\Delta khpA$, $\Delta khpB$ or $\Delta khpA/B$ mutants compared to the $khpA^+/B^+$ wild-type strain, where unchanging MreC amount was used as a loading control (Fig. 8A and B, Supporting Information Figs S13 and S15). In contrast, relative FtsZ amount increased by only \approx 1.5-fold in the $\Delta khpA/B$ mutants (Fig. 8B). The linearity and reproducibility of detection in quantitative Western assays was confirmed for each protein by dilution series (Experimental procedures; Supporting Information Fig. S17). The increase of the relative cellular amounts of FtsA and FtsZ in $\Delta khpA/B$ mutants was similar to that detected for ectopic overexpression of *ftsA* or *ftsZ* respectively (Table 2, lines 3 and 6; Fig. 8B, Supporting Information Figs S14 and S15); but, only overproduction of FtsA, but not FtsZ, suppressed $\Delta pbp2b$ (Table 1, lines, 22–25).

We determined how relative *ftsA* and *ftsZ* transcript amounts tracked with protein amounts. qRT-PCR assays showed that both *ftsA* and *ftsZ* relative transcript amounts increased by \approx 1.5-fold in $\Delta khpA$, $\Delta khpB$ and

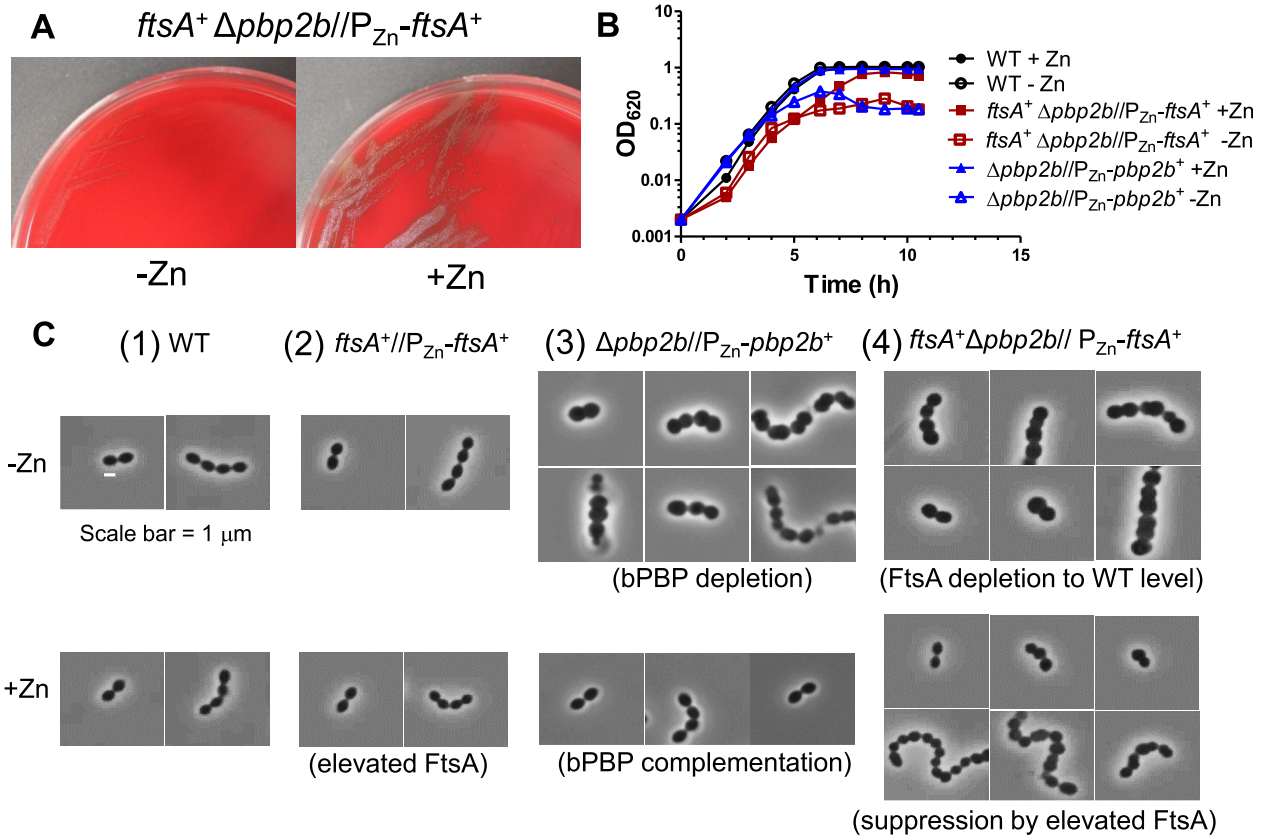


Fig. 7. FtsA overproduction is sufficient to suppress $\Delta pbp2b$.

A. $ftsA^+ \Delta pbp2b/P_{Zn-ftsA^+}$ mutant (IU12707) streaked on TSAII-BA plates lacking (-Zn) or containing (+Zn) 0.5 mM $ZnCl_2$ + 0.05 mM $MnSO_4$. B. Representative growth curves of WT (IU1824) and $\Delta pbp2b/P_{Zn-pbp2b^+}$ (IU11258) and $ftsA^+ \Delta pbp2b/P_{Zn-ftsA^+}$ (IU12707) mutants grown in BHI broth lacking (-Zn) or containing (+Zn) 0.5 mM $ZnCl_2$ + 0.05 mM $MnSO_4$ as described in Experimental procedures. Strain $ftsA^+//P_{Zn-ftsA^+}$ (IU12310) grew similarly to WT with or without Zn (Supporting Information Fig. S16).

C. Representative phase-contrast images of cells of WT (IU1824), $ftsA^+//P_{Zn-ftsA^+}$ (IU12310), $\Delta pbp2b/P_{Zn-pbp2b^+}$ (IU11258) and $ftsA^+ \Delta pbp2b/P_{Zn-ftsA^+}$ (IU12707) strains from growth experiments similar to Fig. 5B sampled at $OD_{620} = 0.1-0.15$.

$\Delta khpA/B$ mutants compared to the wild-type parent (Fig. 8C). Thus, KhpA/B exert a modest degree of negative regulation on $ftsA-ftsZ$ co-transcription that is reflected by a corresponding change in relative FtsZ amount. In contrast, KhpA/B exert negative control that decreases the relative FtsA amount significantly more than the relative transcript amount, which is indicative of post-transcriptional regulation.

The ftsA 5'-UTR is required for FtsA overproduction, which is necessary to suppress $\Delta pbp2b$ in a $\Delta khpA$ mutant

Results presented above show that ectopic overexpression of $ftsA$ is sufficient to suppress $\Delta pbp2b$ (Table 1, line 25; Table 2, line 6). We hypothesized that post-transcriptional induction of FtsA amount is also necessary for $\Delta pbp2b$ suppression in a $\Delta khpA$ mutant. Further, we speculated that this regulation would involve

the 74-nt 5'-UTR leader RNA from the start of $ftsA$ transcription to the start codon of FtsA (Fig. 9A). Consistent with this notion, the mRNA near the start codon of $ftsA$ is preferentially pulled down twofold to threefold by KhpA or KhpB in RIP-Seq experiments, whereas the $ftsZ$ transcript is not pulled down (Supporting Information Fig. S18; Table S4). To test these hypotheses genetically, we constructed merodiploid strains in which the chromosomal copy of $ftsA$ was wild-type or deleted, and $ftsA$ is expressed ectopically from the native P_{ftsA} promoter (entire UTR present) or from the P_{Zn} promoter (Mu *et al.*, 2013) fused to 22 nt from the $czcD$ leader transcript followed by the 24 nt upstream of the FtsA start codon (ΔUTR) (Table 2 and Supporting Information Table S1; Fig. 9A). Production of FtsA solely from ectopic P_{Zn} (+Zn²⁺; ΔUTR) was not sufficient to suppress $\Delta pbp2b$ and did not respond to $\Delta khpA$ (Table 2, lines 7-8). By contrast, production of FtsA solely from ectopic $P_{ftsA}(UTR^+)$ was induced by $\Delta khpA$, thereby suppressing $\Delta pbp2b$ (Table 2, lines 9-10). Last, we

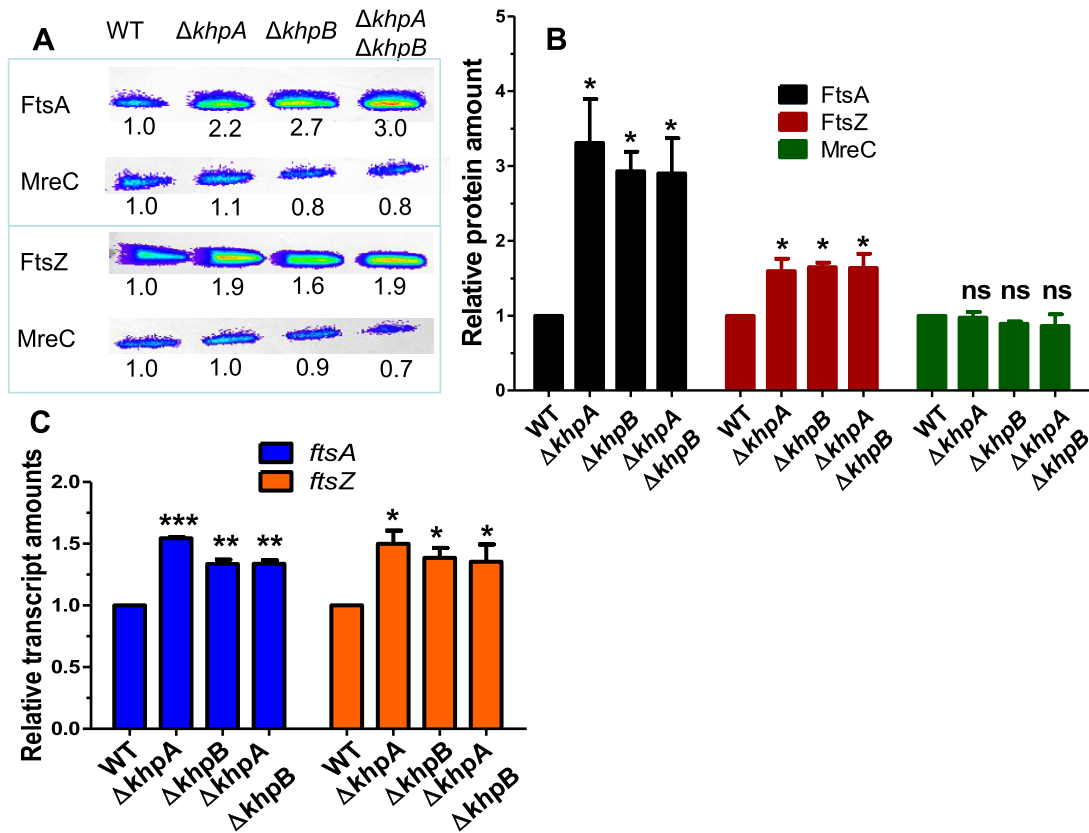


Fig. 8. FtsA amount and to a lesser extent FtsZ amount are negatively regulated by KhpA/B. WT (IU1824) and $\Delta khpA$ (IU9036), $\Delta khpB$ (IU10592) and $\Delta khpA \Delta khpB$ (IU10596) mutants were compared. A. Representative Western blots of cellular amounts of FtsA, FtsZ and MreC (control) in cells growing exponentially in BHI broth. Numbers below lanes are luminescence values relative to WT, determined in the linear range of detection as described in Experimental procedures. B. Average (\pm SE) cellular amounts of FtsA, FtsZ and MreC in mutants relative to WT from three independent experiments. C. Average (\pm SE) relative transcript amounts in mutants relative to WT determined by qRT-PCR from three independent experiments. For B and C, *P* values were obtained relative to WT by one-way ANOVA analysis (GraphPad Prism). **P* < 0.05; ***P* < 0.01; ****P* < 0.001; ns: not significantly different.

constructed the Δ UTR deletion (Δ nt 2–50) in the *ftsA* chromosomal locus (Fig. 9; Table 2, lines 11–12; Supporting Information Table S1). The relative amount of FtsA, but not FtsZ, was reduced by about 50% in the Δ UTR mutant, possibly due to a change in segmental mRNA stability or translation of *ftsA*, and notably, this expression level of FtsA was now insensitive to $\Delta khpA$ (Fig. 9B and C). Together, these results implicate the *ftsA* 5'-UTR in setting the basal amount of the FtsA protein and in the negative regulation of FtsA amount by KhpA/B. They also indicate that FtsA overproduction in $\Delta khpA/B$ mutants is necessary for $\Delta pbp2b$ suppression.

FtsA overproduction only partially accounts for phenotypes of $\Delta khpA$ mutants

Since the relative FtsA amount is induced in $\Delta khpA$, $\Delta khpB$ and $\Delta khpA/B$ mutants (Fig. 8B) and is necessary and sufficient for $\Delta pbp2b$ suppression (Table 2), we tested whether ectopic overexpression of *ftsA* could

account for other phenotypes of $\Delta khpA$ or $\Delta khpB$ mutants (Table 1). Quantitative Western blotting showed that $\Delta khpA$ mutants and *ftsA*⁺//P_{Zn}-*ftsA*⁺ (+Zn²⁺) mero-diploids overproduce cellular FtsA concentrations to comparable levels (Table 2, lines 3 and 6; Supporting Information Figs S13 and S15). Similar to $\Delta pbp2b$, FtsA overproduction suppressed $\Delta mreCD$ and $\Delta rodA$, but surprisingly, did not suppress $\Delta rodZ$ (Table 1, lines 25, 26 and 28), despite RodZ likely playing a role in peripheral PG synthesis (Supporting Information Fig. S1B) (Tsui *et al.*, 2016; Mura *et al.*, 2017). Likewise, increased relative FtsA amount did not suppress $\Delta gpsB$ (Table 1, line 29). As noted previously (Mura *et al.*, 2017), overproduction of FtsA increases *Spn* cell sphericity and decreases relative cell volume slightly, but not nearly as drastically as $\Delta khpA$ (Supporting Information Fig. S16A and S16B). In addition, overexpression of *ftsA* induced the cell-wall stress response mediated by the WalRK TCS (\approx fivefold), but not nearly as strongly as $\Delta khpA/B$ (\approx 12-fold) (Supporting Information

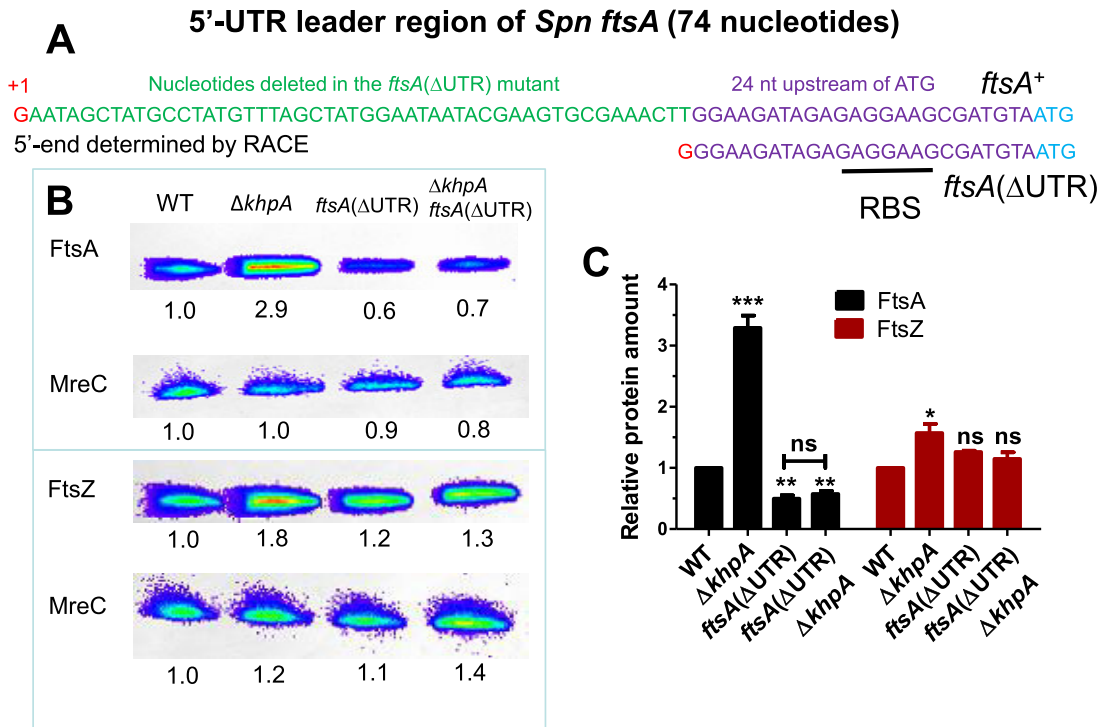


Fig. 9. FtsA induction by the Δ khpA mutation is lost in the absence of an intact 5'-UTR leader of the *ftsA* transcript.

A. Nucleotide (nt) sequence of 74 nt 5'-UTR leader of the *ftsA* transcript. The transcription start site, indicated in red, was determined by 5'-RACE (see Experimental procedures). The 49 nt deleted in the *ftsA*(Δ UTR) mutant are indicated in green. The retained 24 nt containing the RBS upstream of the start codon (ATG) are marked in purple. The same 24 nt was used as the RBS to express FtsA ectopically under control of the P_{zn} promoter (Supporting Information Table S1).

B. Representative Western blots of cellular amounts of FtsA, FtsZ and MreC (control) in WT (IU1824) and Δ khpA (IU9036), *ftsA*(Δ UTR) (IU13641) and Δ khpA *ftsA*(Δ UTR) (IU13672) mutants growing exponentially in BHI broth. Numbers below lanes are luminescence values relative to WT, determined in the linear range of detection as described in Experimental procedures.

C. Average (\pm SE) cellular amounts of FtsA, FtsZ and MreC in mutants relative to WT from three independent experiments. *P* values were obtained relative to WT by one-way ANOVA analysis. * *P* < 0.05; ** *P* < 0.01; *** *P* < 0.001; ns, not significantly different.

Fig. S16C). We conclude that only a subset of phenotypes caused by Δ khpA/B can be accounted for by FtsA overproduction, implying that KhpA/B regulate additional steps in PG synthesis and cell division, besides FtsA concentration (Fig. 10A).

Discussion

In this article, we report the discovery of a complex in cells between two KH-domain RNA-binding proteins, designated as KhpA and KhpB (JAG/EloR), that regulate the cellular amount of the key FtsA cell division protein in *S. pneumoniae*. KhpA is a small single-KH domain protein (Fig. 1A), which have been widely annotated in the genomes of Gram-positive bacteria (Supporting Information Fig. S2). This article is one of the first to report a critical role of a single-KH domain protein in bacterial cell division. By contrast, the conserved KhpB(JAG/EloR) protein contains a 'JAG' domain of unknown function, a large linker region of unknown structure that contains a phosphorylated Thr residue

(T89), and two RNA binding domains (KH and R3H) (Fig. 1B and Supporting Information Fig. S2) (Ulrych *et al.*, 2016; Stamsås *et al.*, 2017). Several results reported here support the conclusion that KhpA and KhpB are RNA binding proteins that interact with each other in the same complex in cells. KhpA and KhpB pull down each other strongly and singularly in reciprocal co-IP experiments (Fig. 3). Δ khpA and Δ khpB mutants phenocopy each other by causing the same growth and cell morphology defects and cell-wall stress response (Figs 2 and 4), and Δ khpA and Δ khpB mutations suppress the same set of mutations deficient in peripheral and general PG synthesis (Table 1), including Δ ppb2b used in the selections that initially identified *khpA* and *khpB*(*eloR*) (Table 1 and Supporting Information Table S2) (Stamsås *et al.*, 2017). Consistent with a KhpA/KhpB complex, KhpA and KhpB co-localize at all stages of cell division (Supporting Information Fig. S8). Finally, KhpA or KhpB separately pulled down a remarkably similar set of mRNA, sRNA, intercistronic RNA and tRNA molecules relative to the untagged control strain

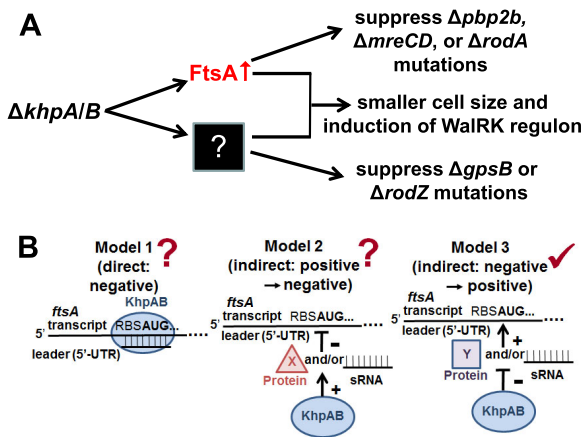


Fig. 10. Models for the regulation of cell division by KhpA and KhpB in *S. pneumoniae* D39.

A. The absence of KhpA or/and KhpB increases cellular FtsA amount, which bypasses the requirement for essential bPBP2b, MreCD and RodA. FtsA overproduction by itself partly contributes to the reduced cell size and induction of the WalRK regulon caused by $\Delta khpA/B$ mutants. In addition, KhpA and KhpB regulate genes other than *ftsA* such that $\Delta khpA/B$ mutants bypass the requirement for essential RodZ and GpsB. See text for details.

B. Three models for how the KhpA/B RNA binding protein could post-transcriptionally regulate FtsA amount via the *ftsA* 5'-UTR leader region. Model 1 and 2 propose direct and indirect models of negative regulation of the *ftsA* 5'-UTR leader, whereas Model 3 is an indirect model wherein KhpA/B negatively regulates the expression or function of an unknown sRNA or protein that positively regulates FtsA production. The mutant analysis in this article favors Model 3 (✓) as discussed in the text, although Models 1 and 2 (?) cannot be ruled out at this point.

in RIP-Seq experiments (Fig. 5, Supporting Information Figs S12 and S18; Supporting Information Table S4). Together, these results support the idea that a multimeric KhpA/KhpB complex functions as a pleiotropic RNA binding protein in the control of PG synthesis and cell division in *S. pneumoniae*.

A Tn-Seq screen previously showed that KhpB and possibly KhpA are virulence factors required for colonization and pneumonia in a murine model of *Spn* TIGR4 infection (van Opijnen and Camilli, 2012). Tn-Seq data were only partially complete for KhpA, possibly because it is a small reading frame. $\Delta khpA$ caused similar phenotypes in encapsulated TIGR4 and D39 (Supporting Information Fig. S3) as in unencapsulated derivatives of D39 (Figs 2 and 4). KhpB was reported independently by three other laboratories. In a chapter of an earlier dissertation not published in a journal, Sauerbier (and Hakenbeck) found that mutant KhpB (and KhpA) imparted increased β -lactam resistance in horizontal gene transfers between *Streptococcus mitis* B6 and *S. pneumoniae* R6 (Sauerbier, 2012). In the D39 background used here, $\Delta khpA/B$ mutants show the same sensitivity as the wild-type strain to penicillin, cefotaxime, piperacillin and tetracycline, but are modestly

resistant to gentamicin in standard disk-diffusion assays (Supporting Information Fig. S19). In addition, this dissertation reported induction of the WalRK TCS regulon in $\Delta khpA$ and $\Delta khpB$ mutants of laboratory strain R6 (Sauerbier, 2012), anticipating the similar results reported here for D39-derived strains (Fig. 4). Induction of the WalRK TCS regulon is necessary for optimal growth of a $\Delta khpA$ mutant, since a $\Delta khpA \Delta walk$ double mutant, lacking Walk histidine kinase, grows much slower than either $\Delta khpA$ or $\Delta walk$ single mutant (Supporting Information Fig. S20).

Recently, Branny, Doubravová and coworkers discovered KhpB, which they named 'JAG', as a substrate of the StkP Ser/Thr protein kinase, which is required for normal *Spn* cell division (Ulrych *et al.*, 2016). In this study, KhpB (JAG) was shown to be phosphorylated on Thr89 and at least one other unknown site in laboratory strain Rx1. In addition, $\Delta khpB(\Delta jag)$ mutations in Rx1 affected *Spn* cell division (Ulrych *et al.*, 2016), and Rx1 $\Delta khpB(\Delta jag)$ mutants showed slower growth rate, reduced cell size (volume), and minimally altered cell shape (aspect ratio), similar to the $\Delta khpA/B$ mutants in the D39 progenitor background (Figs 2 and 4). Induction of an ectopic copy of *khpB⁺(jag⁺)* from the P_{Zn} -inducible promoter in a Rx1 $\Delta khpB(\Delta jag)$ merodiploid strain showed a marginal increase in cell length of $\approx 5\%$ (Ulrych *et al.*, 2016). Similarly, induction of ectopic *khpB⁺(jagG⁺)* (or separately *khpA⁺*) in a D39 Δcps *khpB⁺(jag⁺)* merodiploid strain did not cause substantial cell elongation (Supporting Information Fig. S21).

In a new report, Håvarstein and coworkers independently reported that $\Delta khpB$ suppresses $\Delta bbp2b$ or $\Delta rodA$ in the R704 derivative of laboratory strain R6 (Stamsås *et al.*, 2017). Because of its possible regulatory involvement in peripheral PG elongation, they designated this protein as 'EloR' (Stamsås *et al.*, 2017). In our work, we have retained the name KhpB instead of EloR or JAG, because KhpB interacts with a second RNA binding protein, KhpA and RIP-Seq and mechanistic studies described below show that KhpA/B regulation is not confined to PG elongation.

There are several striking differences between the results reported here in the D39 progenitor background and those reported in the R6 laboratory strain (Stamsås *et al.*, 2017). We showed previously that laboratory strain R6 has accumulated ≈ 80 mutations that are not present in the genetic background of its progenitor D39 strain (Lanie *et al.*, 2007; Rued *et al.*, 2017). In particular, *mreC*, *mreD*, *rodZ* and *gpsB* are not essential in R6 (Straume *et al.*, 2017), whereas they are essential in D39 (Lanie *et al.*, 2007; Land and Winkler, 2011; Rued *et al.*, 2017). Notably, *pbp1a* contains two missense mutations in R6 that are not present in D39 or TIGR4, and we showed previously that swapping the wild-type

allele of *pbp1a* from D39/TIGR4 into R6 restored essentiality of *mreCD* (Land and Winkler, 2011). Hence, the suppression of $\Delta mreCD$, $\Delta rodZ$ and $\Delta gpsB$ by $\Delta khpB(\Delta eloR)$ could not be detected in R6. Similar to R6 (Stamsås *et al.*, 2017), we found that $\Delta khpA/B$ reduce cell aspect ratio slightly ($\approx 10\%$) (Figs 2 and 4); but, we do not interpret this small change as indicative of a major defect in PG elongation that would cause near sphericity (Tsui *et al.*, 2014). By comparison, we reported previously that a D39 *mltG*(Y488D) $\Delta pbp2b$ mutant reduces aspect ratio by $\approx 25\%$, and cells appear spherical (Tsui *et al.*, 2016). The major defect in cell morphology of $\Delta khpA/khpB$ mutants in the progenitor D39 background is an $\approx 50\%$ reduction in cell size (Figs 2 and 4). D39 $\Delta pbp1a$ cells are also significantly smaller than wild-type cells, but have a greater aspect ratio (Land and Winkler, 2011; Tsui *et al.*, 2016). Reduced cell size was described for $\Delta khpB(\Delta jag)$ mutants of strain Rx1 (Ulrych *et al.*, 2016), but was not commented on for R6 $\Delta khpB(\Delta eloR)$ (Stamsås *et al.*, 2017). This large reduction in size is indicative of a reduction in both septal and peripheral PG synthesis in D39 $\Delta khpA/B$ or $\Delta pbp1a$ mutants (Land and Winkler, 2011; Tsui *et al.*, 2016).

Another major difference between the $\Delta khpB$ phenotypes in R6 and D39 is the effect of KhpB T89 phosphorylation by StkP. In R6, a *khpB/eloR*(T89A) phosphoablative change phenocopied $\Delta khpB$, resulting in decreased growth rate, but not suppression of $\Delta pbp2b$ (Stamsås *et al.*, 2017). A *khpB/eloR*(T89E) phosphomimetic mutation was lethal and resulted in the accumulation of *mreC* truncation and *rodZ* null mutations, but surprisingly was not suppressed by $\Delta mreC$ (Stamsås *et al.*, 2017). These results were incorporated into a model in which $\Delta pbp2b$ or $\Delta rodA$ mutations are essential in R6 because of uncontrolled MltG lytic transglycosylase activity, which is reduced by $\Delta khpB(\Delta eloR)$ or absence of T89 phosphorylation (Stamsås *et al.*, 2017). However, in the D39-derived strain IU1824 (Supporting Information Table S1), *khpB*(T89A) does not phenocopy $\Delta khpB$, and *khpB*(T89A), *khpB*(T89D) and *khpB*(T89E) mutants grow like wild-type in the culture conditions tested (Supporting Information Fig. S10). *khpB*(T89A), *khpB*(T89D) and *khpB*(T89E) mutants in D39 derivative IU1824 did not contain suppressor mutations based on whole-genome determinations (see Results). Thus, phosphorylation of KhpB at Thr89 does not affect KhpB function in the D39 progenitor background. A possible role of the second phosphorylation site in KhpB remains to be explored (Ulrych *et al.*, 2016; Stamsås *et al.*, 2017).

We reported previously that the *mltG*(Y488D) mutation, which likely reduces the activity of the essential MltG endo-lytic transglycosylase, suppresses the

requirement for peripheral PG synthesis in D39, with some restrictions (Tsui *et al.*, 2016). The model that peripheral PG genes are essential simply because of uncontrolled MltG activity (Stamsås *et al.*, 2017) is not readily reconciled with the combinations of mutations that are synthetically viable in D39 or the suppression of $\Delta mltG$ by spontaneous mutations that inactivate *pbp1a* (Tsui *et al.*, 2016). The differences in the phenotypes in response to KhpB phosphorylation at Thr89 in R6 versus D39 may reflect the bypass mechanism accumulated by laboratory strain R6 that is not present in the virulent D39 progenitor strain. Finally, the mechanism for the suppression of $\Delta pbp2b$ by $\Delta khpA/B$ in D39 described next only indirectly involves regulation of PG elongation.

Overproduction of FtsA as a possible mechanism of $\Delta pbp2b$ suppression was first hinted at by isolation of a suppressor mutant that contained only a tandem chromosomal duplication of the *ftsA-ftsZ* chromosomal region (Fig. 6; Supporting Information Table S2). We showed that ectopic overexpression of *ftsA* alone is sufficient to suppress $\Delta pbp2b$, $\Delta mreCD$ and $\Delta rodA$ (Tables 1 and 2; Figs 7 and 10A). Overproduction of FtsA also partly can account for the smaller cell size and induction of the WalRK TCS cell-wall stress regulon in $\Delta khpA/B$ mutants (Fig. 10A and Supporting Information Fig. S16). Consistent with overproduction of FtsA as the mechanism of $\Delta pbp2b$ suppression, the cellular concentration of FtsA is \approx threefold greater in $\Delta khpA/B$ mutants than in the wild-type parent strain (Fig. 8; Table 2). There is a smaller (≈ 1.5 -fold) increase in the relative amount of FtsZ as well. Consistent with results from Western blotting, comparable increases in the relative cellular amounts of FtsA and FtsZ were independently detected by quantitative MS-based (tandem-mass tag; TMT) proteomics of a $\Delta khpA \Delta khpB$ mutant compared to the parent strain (data not shown). In contrast to relative protein amounts, the relative amounts of both the *ftsA* and *ftsZ* transcripts increased by the same amount (≈ 1.5 -fold) in the $\Delta khpA/B$ mutants compared to the parent (Fig. 8), indicating that part of the increase in relative FtsA protein amount is exerted at the post-transcriptional level. The increase in relative FtsA amount in $\Delta khpA/B$ mutants is comparable to that attained by ectopic *ftsA* overexpression that suppresses $\Delta pbp2b$ (Table 2). FtsA is a highly abundant protein in *Spn* cells (Lara *et al.*, 2005), and there may be unknown negative feedback regulatory mechanisms that modulate FtsA amount during the cell cycle and set a limit for the level of FtsA overproduction that can be attained.

Post-transcriptional regulation of FtsA amount pointed to the 74-nt 5'-UTR leader of the *ftsA-ftsZ* operon (Fig. 9A) as a possible site of regulation mediated by KhpA/B. In testing this hypothesis, we were able to

demonstrate that overproduction of FtsA is necessary, as well as sufficient for suppression of $\Delta pbb2b$. Using both ectopic constructs and a chromosomal deletion mutation, we found that overproduction of FtsA in cells in response to the absence of KhpA depends on an intact *ftsA* 5'-UTR leader region (Fig. 9; Table 2). In particular, the relative amount of FtsA, but not FtsZ, was reduced by about 50% in the chromosomal deletion of the *ftsA* 5'-UTR leader (Δ UTR), possibly due to a change in segmental mRNA stability or translation initiation of *ftsA*; but, now the expression level of FtsA was insensitive to $\Delta khpA$ (Fig. 9). Three general models for regulation of relative FtsA amount by KhpA/B are presented in Fig. 10B. In model 1, *ftsA* translation is negatively regulated by binding to a sRNA in the presence of KhpA/B; alternatively, KhpA/B could act as a direct negative regulator by binding to the *ftsA* 5'-UTR leader (not shown). Model 2 invokes indirect positive regulation by KhpA/B of a negative regulator (sRNA or protein) of *ftsA* translation. Model 3 is based on indirect negative regulation by KhpA/B of a positive regulator (sRNA or protein) of *ftsA* translation. At this point, we know that an intact *ftsA* 5'-UTR leader is required for increased FtsA production in the absence of KhpA/B (Fig. 9; Table 2); but, this result does not distinguish among these models. mRNA near the *ftsA* 5'-UTR and start codon is preferentially pulled down by KhpA or KhpB in RIP-Seq experiments (Supporting Information Fig. S18; Table S4), which would tend to support model 1. Conversely, we know that the chromosomal *ftsA*(Δ UTR) mutation reduces relative basal amount of FtsA, without changing relative FtsZ amount, where *ftsA-ftsZ* are co-transcribed (Figs 6 and 9). The reduced relative basal amount of FtsA in the *ftsA*(Δ UTR) mutant might suggest loss of a positive regulator of *ftsA* translation, as proposed for model 3. However, the *ftsA*(Δ UTR) mutation could change intrastrand mRNA pairing or locally destabilize the *ftsA* mRNA in the RBS region without affecting the stability of downstream *ftsZ* mRNA. Additional work is needed to determine the mechanism of *ftsA* regulation by KhpA/B.

The mechanism of how FtsA overproduction suppresses $\Delta pbb2b$, $\Delta mreCD$ and $\Delta rodA$ mutations also remains to be determined (Fig. 10A). FtsA is a membrane-associated actin homologue that anchors the FtsZ ring to the cell membrane (Juarez and Margolin, 2012; Lutkenhaus *et al.*, 2012; Busiek and Margolin, 2015; Ortiz *et al.*, 2016). FtsA is essential in ovoid-shaped bacteria, like *Spn*, and has different properties than in rod-shaped bacteria [see (Mura *et al.*, 2017)]. In particular, FtsA plays roles in maintaining coherent FtsZ rings and coordinating peripheral and septal PG synthesis from the midcell region of *Spn* cell (Supporting Information Fig. S1A) (Mura *et al.*, 2017). These regulatory

roles require interactions of FtsA with other septation and elongation proteins (Lutkenhaus *et al.*, 2012; Busiek and Margolin, 2015; Du *et al.*, 2016; Ortiz *et al.*, 2016). It has been speculated that *Spn* FtsA may even assume similar functions in midcell peripheral PG synthesis as MreB, which mediates side-wall PG synthesis in rod-shaped bacteria and is absent in *Spn* (Supporting Information Fig. S1B) (Massidda *et al.*, 2013; Mura *et al.*, 2017). It is notable that FtsA overproduction in wild-type *Spn* cells stimulates septation and leads to smaller cells (Mura *et al.*, 2017). Therefore, excess FtsA may speed up cell closure sufficiently that the requirement for full peripheral elongation diminishes. Another non-exclusive possibility is that overproduced FtsA may recruit or alter the activities of other PBPs to compensate for the absence of bPBP2b, MreCD and RodA from the peripheral PG synthesis machine. Both of these mechanisms would result in the characteristic decrease in cell length, width and size, but only slightly decreased ovoid shape of $\Delta khpA/B$ mutants (Figs 2 and 4) (Ulrych *et al.*, 2016). Further studies of the role of FtsA in coordinating septal and peripheral PG synthesis in *Spn* may shed light onto the suppression mechanism [see (Mura *et al.*, 2017)].

Finally, several pieces of evidence indicate that KhpA/B regulate genes other than *ftsA* in *Spn*. Most tellingly, excess FtsA amount did not suppress $\Delta gpsB$ or $\Delta rodZ$ (Table 1; Fig. 10A). Lack of suppression of $\Delta rodZ$ is curious, because RodZ is thought to function primarily in peripheral PG synthesis (Gerdes, 2009; van den Ent *et al.*, 2010; Shiomi *et al.*, 2013; Tsui *et al.*, 2016;), in contrast to GpsB whose function is not confined to this process (Land *et al.*, 2013; Fleurie *et al.*, 2014; Rismondo *et al.*, 2016; Rued *et al.*, 2017). This shared lack of suppression suggests that $\Delta khpA/B$ changes the expression of other genes besides *ftsA* and that RodZ could play a role in mediating GpsB function in septal and peripheral PG synthesis (Fleurie *et al.*, 2014; Tsui *et al.*, 2016; Rued *et al.*, 2017). Regulation of multiple pathways by KhpA/B is supported by results from RIP-Seq (Fig. 5; Supporting Information Table S4) and initial quantitative TMT-MS proteomics (data not shown), where multiple RNAs are pulled down by KhpA/B in RIP-Seq and relative amounts of numerous proteins change in $\Delta khpA/B$ mutants compared to the parent strain. Current efforts are underway to compare and reconcile these RNA and protein data sets.

Regulation by KhpA/B likely occurs predominantly at the post-transcriptional level, since only the relative transcript amounts of genes in the WalRK TCS cell-wall stress regulon strongly change in $\Delta khpA/B$ mutants (Figs 2 and 4; Supporting Information Table S3) (Sauerbier, 2012). The hypothesis that widely distributed KhpA and KhpB (Supporting Information Fig. S2) form a multimeric RNA chaperone complex could address a

long-standing issue in Gram-positive RNA biology. Hfq plays an indispensable regulatory role in Gram-negative bacteria (De Lay *et al.*, 2013; Van Assche *et al.*, 2015; Feliciano *et al.*, 2016; Updegrave *et al.*, 2016), whereas the roles played by Gram-positive Hfq homologues remain 'elusive' (Rochat *et al.*, 2012, 2015; Bouloc and Repoila, 2016; Keefer *et al.*, 2017). Moreover, Hfq homologues are missing from many Gram-positive species, including *S. pneumoniae* (Lanie *et al.*, 2007). We speculate that a KhpA/B multimeric complex may act redundantly in Gram-positive species containing Hfq and fulfill the role of an RNA chaperone in those species that lack an Hfq homologue. The hypothesis that KhpA/B is a multimeric complex that acts as a general RNA chaperone requires future testing.

Experimental procedures

Bacterial strains and growth conditions

Strains used in this study are listed in Supporting Information Table S1. All strains were derived from strain IU1824 (D39 Δcps *rpsL1*), IU1945 (D39 Δcps) or encapsulated serotype 2 strain D39 strain IU1690 (Lanie *et al.*, 2007). Strains containing antibiotic markers were constructed by transformation of competent pneumococcal cells with linear DNA amplicons synthesized by overlapping fusion PCR (Ramos-Montañez *et al.*, 2008; Tsui *et al.*, 2010; 2016). Strains containing markerless alleles in native chromosomal loci were constructed using allele replacement via the P_c -[*kan-rpsL*⁺] (Janus cassette) (Sung *et al.*, 2001). Primers used to synthesize different amplicons are listed in Supporting Information Table S1. Bacteria were grown on plates containing trypticase soy agar II (modified; Becton-Dickinson) and 5% (vol/vol) defibrinated sheep blood (TSAll-BA). Plates were incubated at 37°C in an atmosphere of 5% CO₂. TSAll-BA plates for selections contained antibiotics at concentrations described previously (Tsui *et al.*, 2010, 2016). Bacteria were cultured statically in Becton-Dickinson brain heart infusion (BHI) broth at 37°C in an atmosphere of 5% CO₂, and growth was monitored by OD₆₂₀ as described before (Tsui *et al.*, 2016). Mutant constructs were confirmed by PCR and DNA sequencing of chromosomal regions corresponding to the amplicon region used for transformation.

In all experiments, cells were inoculated from frozen glycerol stocks into BHI broth, serially diluted and incubated 12–16 h statically at 37°C in an atmosphere of 5% CO₂. 0.5 mM ZnCl₂ + 0.05 mM MnSO₄ (+Zn) was added to BHI broth cultures of merodiploid strains that require Zn²⁺ for growth due to ectopic expression of an essential gene (i.e., IU11258, IU12707, IU12901 and IU12959) (Tsui *et al.*, 2016). The next day, cultures at OD₆₂₀ ≈ 0.05–0.4 were diluted to OD₆₂₀ ≈ 0.002 in BHI broth lacking (–Zn) or containing (+Zn) 0.5 mM ZnCl₂ + 0.05 mM MnSO₄ and cultured under the same conditions. Cultures were sampled in early to mid-exponential phase for different experiments as indicated. For depletion experiments, overnight cultures of

Zn²⁺-requiring merodiploid strains were centrifuged once to remove the +Zn medium and resuspended ($t = 0$ in growth curves) in BHI broth lacking (–Zn) or containing (+Zn) 0.5 mM ZnCl₂ + 0.05 mM MnSO₄.

Transformation assays

Transformations were performed as previously described (Tsui *et al.*, 2016; Rued *et al.*, 2017). $\Delta pbp2b$ <>*aad9*, $\Delta pbp2b$ <> P_c -*erm*, $\Delta rodA$:: P_c -*erm*, $\Delta mreCD$ <>*aad9*, $\Delta cozE$:: P_c -*erm*, $\Delta mltG$:: P_c -*erm*, $\Delta rodZ$ <>*aad9* and $\Delta gpsB$ <>*aad* amplicons, and a $\Delta pbp1b$:: P_c -*erm* amplicon used as a positive control each contained ≈ 1 kb of flanking chromosomal DNA. Amplicons were synthesized by PCR using the primers and templates listed in Supporting Information Table S1.

Whole-genome DNA sequencing

Whole-genome sequencing was used to identify suppressor mutations and to verify the genomes of constructed mutants. Strains IU7476 and IU12015 containing suppressor mutations that allowed growth of a $\Delta pbp2b$ mutant were isolated as described previously before (Tsui *et al.*, 2016; Rued *et al.*, 2017). Mutants *khpB*(T89A) (IU12744; IU13885), *khpB*(T89D), (IU13881; IU13887) or *khpB*(T89E) (IU13883; IU13889) were constructed and isolated from independent transformation reactions as described in Supporting Information Table S1. Genomic DNA preparation, DNA library construction, Illumina MiSeq or NextSeq DNA sequencing, and bioinformatics analyses were performed as described previously (Tsui *et al.*, 2016; Rued *et al.*, 2017). The number of reads of each base was mapped to the D39 reference genome using the JBrowse program (Skinner *et al.*, 2009; Westesson *et al.*, 2013) to detect regions containing chromosomal duplications or large deletions (Rued *et al.*, 2017).

We explicitly determined the nature of the duplication containing *ftsA-ftsZ* at 1,492,424 through 1,500,342 (Fig. 6) as follows. After the initial bowtie analysis, we identified all the reads that were not mapped to the genome. These reads were then re-aligned using bowtie with the addition of the –local option. Reads locally mapped to the region of the deletion were then manually examined and re-aligned to the entire genome using NCBI Blastn. Reads spanning the junction between the 3' end of the putative repeat region to the 5' end of the repeat region were identified which is consistent with the hypothesis that the repeat was a tandem duplication that occurred in place without any other obvious re-arrangements taking place. The coverage is consistent with this being a single duplication event.

Cell length and width measurements

Cell lengths and widths of strain growing exponentially in BHI broth were measured as previously described (Tsui *et al.*, 2016). More than 100 cells from at least two independent experiments were measured, and *P* values were

obtained by one-way ANOVA analysis using the GraphPad Prism program.

RNA preparation, mRNA-Seq and qRT-PCR

RNA preparation, qRT-PCR and mRNA-Seq analyses of transcripts >200 nt were performed as previously described (Tsui *et al.*, 2016; Zheng *et al.*, 2016). Primers used for qRT-PCR are listed in Supporting Information Table S1. mRNA-Seq data are deposited in the GEO database (accession number GSE101583).

Co-immunoprecipitation

IU1945 (WT), IU9602 (*khpA*-L-FLAG³) and IU10664 (*khpB*-L-FLAG³) strains were treated with formaldehyde cross linker, and FLAG-tagged proteins were used as bait for co-IP using anti-FLAG magnetic beads as described previously (Rued *et al.*, 2017). Eluted protein samples were mixed with same volume of 2X Laemmli sample buffer (Bio-Rad) containing 5% (vol/vol) β -mercaptoethanol (Sigma) and heated at 95°C for 1 h to break crosslinks. Twenty microliter of each sample were separated by SDS-PAGE on 4%–15% precast protein gels (Bio-Rad) in Tris-glycine buffer. Gels were treated with Pierce silver stain for MS (ThermoFisher) according to the manufacturer's protocol. Prey bands were cut from gels, destained, trypsin digested and identified by MS at the IUB core facility (Sham *et al.*, 2011).

KhpA and KhpB structure modeling

The aa sequences of KhpA and KhpB were entered into the SWISS-Model server (Arnold *et al.*, 2006). The PDB numbers of the templates for modeling the structures of KhpA and KhpB were 4V6W (KH domain from *Drosophila melanogaster* 80S ribosome) and 3GKU (KhpB homologue of *Clostridium symbiosum*) respectively. The resulting PDB models were visualized and aligned in PyMOL (The PyMOL Molecular Graphics System; Version 1.7.4.3; Schrödinger, LLC 2; www.pymol.org).

Quantitative Western blotting

Western blotting was performed as previously described (Wayne *et al.*, 2010; Tsui *et al.*, 2014; Zheng *et al.*, 2016). Cell lysates were prepared by the FastPrep homogenizer method described before (Wayne *et al.*, 2010; Tsui *et al.*, 2014; Zheng *et al.*, 2016). Protein concentrations were determined with the DCTM protein assay (Bio-Rad), and equal amounts of protein (2.5 μ g) were loaded into each lane on duplicate SDS-PAGE gels. After transfer of proteins from a gel to a membrane, the membrane was cut into two sections, such that the upper section contained FtsA (50 kDa) or FtsZ (45 kDa) and the low section contained MreC (30 kDa) as a loading and blotting control. The separated membranes were labeled with anti-FtsA (1:10,000), anti-FtsZ (1:10,000) or anti-MreC (1:5,000) as primary antibodies for immunodetection (Lara *et al.*, 2005; Land and Winkler, 2011). Chemiluminescence of protein bands in

Western blots was quantitated using an IVIS imaging system as described previously (Wayne *et al.*, 2010). To check the linearity of signal intensity versus protein amount, cell lysates from the WT strain (IU1824) were serially diluted, and different amounts of total lysate protein (1.25, 2.50, 5.00 and 10.0 μ g) were subjected to Western blotting with detection using anti-FtsA, anti-FtsZ or anti-MreC antibodies. The signal intensity obtained for each band was linear with the amount of each protein loaded (Supporting Information Fig. S17), confirming the linearity and reproducibility of detection of the quantitative Western blot assay. Western blotting to detect phosphorylated *Spn* proteins using anti-phosphothreonine (anti-pThr) antibody was performed as described previously (Rued *et al.*, 2017).

Two-dimensional immunofluorescence microscopy (IFM)

Co-localization of FLAG-tagged KhpA and HA-tagged KhpB was performed by IFM as described before (Land *et al.*, 2013; Tsui *et al.*, 2014) in exponentially growing cells of strain IU10602 (*khpA*-L-FLAG³ *khpB*-HA). Two-dimensional IFM images were averaged and quantitated using a previously described graphical user interface (GUI) program (Land *et al.*, 2013). Demographs of protein localization were generated using the MicrobeJ program (Ducret *et al.*, 2016).

5'-Rapid amplification of cDNA ends (RACE)

The transcription start site of *ftsA*-*ftsZ* mRNA in wild-type cells growing exponentially in BHI broth was determined by the SMARTer-RACE 5'/3' kit (Clontech) according to the manufacturer's instructions.

RNA immunoprecipitation and sequencing (RIP-Seq)

Bacterial RIP-Seq was carried out by a modification of a previously published method (Saadeh *et al.*, 2015). The method of recovery of FLAG-tagged bait proteins bound to cellular RNAs was similar to that used for co-IP described above (Rued *et al.*, 2017), except that there was no formaldehyde crosslinking and glycine quenching steps. Briefly, strains IU1945 (WT), IU9602 (*khpA*-L-FLAG³) and IU10664 (*khpB*-L-FLAG³) were grown in 400 ml of BHI broth to OD₆₂₀ \approx 0.25–0.40. Cells were collected by centrifugation (8,000 \times *g* for 10 min at 4°C). Cell pellets were washed once with 30 ml of cold 1XPBS (4°C) and resuspended in 2 ml of cold lysis buffer (50 mM Tris-HCl pH 7.4, 150 mM NaCl, 1% Triton X100 (v/v) containing protease inhibitor (ThermoFisher; cat#78429)). Suspensions (2 ml) were transferred into two lysing matrix B tubes (1 ml each) (MB Biomedicals, Inc.). Tubes were shaken in a FastPrep homogenizer at 4°C for ten 40s cycles (4 \times shaking; 5 min on ice; 3 \times shaking; 5 min on ice; 3 \times shaking) at a setting of 6.0 M/s. Cell debris was removed by centrifuging at 16,000 \times *g* for 5 min at 4°C. Protein concentration was determined by DCTM protein assay (Bio-Rad). About 1 ml of lysate with similar protein amount was added to tubes with 50 μ l of anti-FLAG magnetic beads (Sigma) and

rotated for 2 h at 4°C. The beads were washed three times with 1 ml of lysis buffer for 10 min with rotation at 4°C. FLAG³-tagged protein bound to RNA was eluted by incubation with 100 µl of FLAG elution solution (150 ng of 3× FLAG peptide per µl) (Sigma) for 30 min at 4°C.

RNA was extracted by phenol-chloroform extraction. Hundred microliter of phenol/chloroform/isoamyl alcohol (125:24:1, pH 4.3, ThermoFisher) was added to the eluted solution and vortexed for 10 sec before incubation at room temperature for 5 min. The mixture was centrifuged at 16,000 × *g* for 5 min. The upper phase was transferred to a new 1.5 ml tube. Two volume of isopropanol and 1/10 volume of 3 M sodium acetate (pH 5.2) was added, followed by incubation for 10 min at −80°C to precipitate RNA. Precipitated material was collected by centrifugation (16,000 × *g* for 30 min, 4°C) and washed with 500 µl of 80% ethanol. Pellets were dried at room temperature for 10 min and resuspended in 30 µl of nuclease-free water. RNA was sequenced as described before for mRNA-Seq experiments (Tsui *et al.*, 2016; Zheng *et al.*, 2016). A ratio of reads for an RNA species greater than fourfold between the FLAG-tagged KhpA or KhpB sample and the non-FLAG-tagged control sample (IU1945) was considered indicative of a possible interaction between the RNA and KhpA or KhpB (Saadeh *et al.*, 2015). The number of reads of each base was mapped to the D39 reference genome using the JBrowse program (Skinner *et al.*, 2009; Westesson *et al.*, 2013) as described above. RIP-Seq data are deposited in the GEO database (accession number GSE103735).

Disk diffusion assay for antibiotic resistance

Disk diffusion assays were performed as described before (Zheng *et al.*, 2016). Antibiotic disks were purchased from Becton, Dickinson and Co. Disks used in assays were penicillin (10 U), cefotaxime (30 µg), piperacillin (100 µg), tetracycline (30 µg) and gentamicin (120 µg).

Acknowledgements

We thank Dhriti Sinha, Kevin Bruce and Eric Kim for methods and constructed bacterial strains, other members of the Winkler laboratory for critical comments and discussions, Jesus Bazan, James Ford, Kurt Zimmer, Ram Podicheti and Doug Rusch for assistance with genomic methods and bioinformatics, and Jon Trinidad for MS identifications and preliminary TMT experiments. This work was supported by NIH grant RO1GM113172 and NIH grant RO1GM114315 (to M.E.W.), and by LR7/2007 grant CRP2–401 from the Autonomous Region of Sardinia (RAS) (to O.M.).

Author contributions

Conception or design of the study (JJZ, HCTT, MEW); acquisition, analysis or interpretation of data (JJZ, AJP, HCTT, OM, MEW); writing the manuscript (JJZ, AJP, HCTT, OM, MEW).

References

- Arnold, K., Bordoli, L., Kopp, J., and Schwede, T. (2006) The SWISS-MODEL Workspace: a web-based environment for protein structure homology modelling. *Bioinformatics* **22**: 195–201.
- Barendt, S.M., Sham, L.T., and Winkler, M.E. (2011) Characterization of mutants deficient in the L,D-carboxypeptidase (DacB) and WalRK (VicRK) regulon, involved in peptidoglycan maturation of *Streptococcus pneumoniae* serotype 2 strain D39. *J Bacteriol* **193**: 2290–2300.
- Beilharz, K., Nováková, L., Fadda, D., Branny, P., Massidda, O., and Veening, J.W. (2012) Control of cell division in *Streptococcus pneumoniae* by the conserved Ser/Thr protein kinase StkP. *Proc Natl Acad Sci USA* **109**: E905–E913.
- Bendezu, F.O., and de Boer, P.A. (2008) Conditional lethality, division defects, membrane involution, and endocytosis in *mre* and *mrd* shape mutants of *Escherichia coli*. *J Bacteriol* **190**: 1792–1811.
- Berg, K.H., Stamsås, G.A., Straume, D., and Håvarstein, L.S. (2013) Effects of low PBP2b levels on cell morphology and peptidoglycan composition in *Streptococcus pneumoniae* R6. *J Bacteriol* **195**: 4342–4354.
- Boersma, M.J., Kuru, E., Rittichier, J.T., VanNieuwenhze, M.S., Brun, Y.V., and Winkler, M.E. (2015) Minimal Peptidoglycan (PG) Turnover in wild-type and PG hydrolase and cell division mutants of *Streptococcus pneumoniae* D39 growing planktonically and in host-relevant biofilms. *J Bacteriol* **197**: 3472–3485.
- Boulloc, P., and Repoila, F. (2016) Fresh layers of RNA-mediated regulation in Gram-positive bacteria. *Curr Opin Microbiol* **30**: 30–35.
- Brown, J., S., Hammerschmidt, C.J. and Orihuela, (2015) *Streptococcus pneumoniae Molecular Mechanisms of Host-Pathogen Interactions*. London, UK: Academic Press.
- Busiek, K.K., and Margolin, W. (2015) Bacterial actin and tubulin homologs in cell growth and division. *Curr Biol: CB* **25**: R243–R254.
- CDC. (2013) *Antibiotic resistance threats in the United States*. [WWW document]. URL <http://www.cdc.gov/drugresistance/threat-report-2013/>
- De Lay, N., Schu, D.J., and Gottesman, S. (2013) Bacterial small RNA-based negative regulation: Hfq and its accomplices. *J Biol Chem* **288**: 7996–8003.
- Du, S., Pichoff, S., and Lutkenhaus, J. (2016) FtsEX acts on FtsA to regulate divisome assembly and activity. *Proc Natl Acad Sci USA* **113**: E5052–E5061.
- Dubrac, S., Bisicchia, P., Devine, K.M., and Msadek, T. (2008) A matter of life and death: cell wall homeostasis and the WalkR (YycGF) essential signal transduction pathway. *Mol Microbiol* **70**: 1307–1322.
- Ducret, A., Quardokus, E.M., and Brun, Y.V. (2016) MicrobeJ, a tool for high throughput bacterial cell detection and quantitative analysis. *Nat Microbiol* **1**: 16077.
- van den Ent, F., Johnson, C.M., Persons, L., de Boer, P., and Lowe, J. (2010) Bacterial actin MreB assembles in complex with cell shape protein RodZ. *EMBO J* **29**: 1081–1090.
- Egan, A.J., Biboy, J., van't Veer, I., Breukink, E., and Vollmer, W. (2015) Activities and regulation of

- peptidoglycan synthases. *Philos Trans Royal Soc Lond B, Biol Sci* **370**: pii.20150031.
- Egan, A.J.F., Cleverley, R.M., Peters, K., Lewis, R.J., and Vollmer, W. (2017) Regulation of bacterial cell wall growth. *FEBS J* **284**: 851–867.
- Feliciano, J.R., Grilo, A.M., Guerreiro, S.I., Sousa, S.A., and Leitao, J.H. (2016) Hfq: a multifaceted RNA chaperone involved in virulence. *Future Microbiol* **11**: 137–151.
- Fenton, A.K., Mortaji, L.E., Lau, D.T., Rudner, D.Z., and Bernhardt, T.G. (2016) CozE is a member of the MreCD complex that directs cell elongation in *Streptococcus pneumoniae*. *Nat Microbiol* **2**: 16237.
- Ferreira, D.M., and Gordon, S.P. (2015) Mechanisms causing inflammatory response to *Streptococcus pneumoniae*. In *Streptococcus pneumoniae Molecular Mechanisms of Host-Pathogen Interactions*. Brown, J., Hammerschmidt, S., and Orihuela, C.J. (eds.). London, UK: Academic Press, pp. 383–400.
- Fleurie, A., Manuse, S., Zhao, C., Campo, N., Cluzel, C., Lavergne, J.P., et al. (2014) Interplay of the serine/threonine-kinase StkP and the paralogs DivIVA and GpsB in pneumococcal cell elongation and division. *PLoS Genet* **10**: e1004275.
- Fritz, G., and Mascher, T. (2014) A balancing act times two: sensing and regulating cell envelope homeostasis in *Bacillus subtilis*. *Mol Microbiol* **94**: 1201–1207.
- Gerdes, K. (2009) RodZ, a new player in bacterial cell morphogenesis. *EMBO J* **28**: 171–172.
- Gratz, N., Loh, L.N., and Tuomanen, E.I. (2015) Pneumococcal invasion: development of bacteremia and meningitis. In *Streptococcus pneumoniae Molecular Mechanisms of Host-Pathogen Interactions*. Brown, J., Hammerschmidt, S., and Orihuela, C.J. (eds.). London, UK: Academic Press, pp. 433–451.
- Gutu, A.D., Wayne, K.J., Sham, L.T., and Winkler, M.E. (2010) Kinetic characterization of the WalRKSpn (VicRK) two-component system of *Streptococcus pneumoniae*: dependence of WalKSpn (VicK) phosphatase activity on its PAS domain. *J Bacteriol* **192**: 2346–2358.
- Hakenbeck, R., Bruckner, R., Denapaite, D., and Maurer, P. (2012) Molecular mechanisms of beta-lactam resistance in *Streptococcus pneumoniae*. *Future Microbiol* **7**: 395–410.
- Henriques-Normark, B., and Tuomanen, E.I. (2013) The pneumococcus: epidemiology, microbiology, and pathogenesis. *Cold Spring Harb Perspect Med* **3**: pii.a010215.
- Iovino, F., Seinen, J., Henriques-Normark, B., and van Dijk, J.M. (2016) How does *Streptococcus pneumoniae* invade the brain? *Trends Microbiol* **24**: 307–315.
- Jacobsen, F.E., Kazmierczak, K.M., Lisher, J.P., Winkler, M.E., and Giedroc, D.P. (2011) Interplay between manganese and zinc homeostasis in the human pathogen *Streptococcus pneumoniae*. *Metallomics* **3**: 38–41.
- Jacq, M., Adam, V., Bourgeois, D., Moriscot, C., Di Guilmi, A.M., Vernet, T., and Morlot, C. (2015) Remodeling of the Z-Ring Nanostructure during the *Streptococcus pneumoniae* cell cycle revealed by photoactivated localization microscopy. *mBio* **6**: pii.e01108-15.
- Juarez, J.R., and Margolin, W. (2012) A bacterial actin unites to divide bacterial cells. *EMBO J* **31**: 2235–2236.
- Keefer, A.B., Asare, E.K., Pomerantsev, A.P., Moayeri, M., Martens, C., Porcella, S.F., et al. (2017) In vivo characterization of an Hfq protein encoded by the *Bacillus anthracis* virulence plasmid pXO1. *BMC Microbiol* **17**: 63.
- Land, A.D., and Winkler, M.E. (2011) The requirement for pneumococcal MreC and MreD is relieved by inactivation of the gene encoding PBP1a. *J Bacteriol* **193**: 4166–4179.
- Land, A.D., Tsui, H.C., Kocaoglu, O., Vella, S.A., Shaw, S.L., Keen, S.K., et al. (2013) Requirement of essential Pbp2x and GpsB for septal ring closure in *Streptococcus pneumoniae* D39. *Mol Microbiol* **90**: 939–955.
- Lanie, J.A., Ng, W.L., Kazmierczak, K.M., Andrzejewski, T.M., Davidsen, T.M., Wayne, K.J., et al. (2007) Genome sequence of Avery's virulent serotype 2 strain D39 of *Streptococcus pneumoniae* and comparison with that of unencapsulated laboratory strain R6. *J Bacteriol* **189**: 38–51.
- Lara, B., Rico, A.I., Petruzzelli, S., Santona, A., Dumas, J., Biton, J., et al. (2005) Cell division in cocci: localization and properties of the *Streptococcus pneumoniae* FtsA protein. *Mol Microbiol* **55**: 699–711.
- Leclercq, S., Derouaux, A., Olatunji, S., Fraipont, C., Egan, A.J., Vollmer, W., et al. (2017) Interplay between penicillin-binding proteins and SEDS proteins promotes bacterial cell wall synthesis. *Sci Rep* **7**: 43306.
- Lutkenhaus, J., Pichoff, S., and Du, S. (2012) Bacterial cytokinesis: from Z ring to divisome. *Cytoskeleton (Hoboken)* **69**: 778–790.
- Martin, J.E., Edmonds, K.A., Bruce, K.E., Campanello, G.C., Eijkelkamp, B.A., Brazel, E.B., et al. (2017a) The zinc efflux activator SczA protects *Streptococcus pneumoniae* serotype 2 D39 from intracellular zinc toxicity. *Mol Microbiol* **104**: 636–651.
- Martin, J.E., Lisher, J.P., Winkler, M.E., and Giedroc, D.P. (2017b) Perturbation of manganese metabolism disrupts cell division in *Streptococcus pneumoniae*. *Mol Microbiol* **104**: 334–348.
- Massidda, O., Novakova, L., and Vollmer, W. (2013) From models to pathogens: how much have we learned about *Streptococcus pneumoniae* cell division? *Environ Microbiol* **15**: 3133–3157.
- Meeske, A.J., Riley, E.P., Robins, W.P., Uehara, T., Mekalanos, J.J., Kahne, D., et al. (2016) SEDS proteins are a widespread family of bacterial cell wall polymerases. *Nature* **537**: 634–638.
- Morlot, C., Bayle, L., Jacq, M., Fleurie, A., Tourcier, G., Galisson, F., et al. (2013) Interaction of Penicillin-Binding Protein 2x and Ser/Thr protein kinase StkP, two key players in *Streptococcus pneumoniae* R6 morphogenesis. *Mol Microbiol* **90**: 88–102.
- Mu, D., Montalban-Lopez, M., Masuda, Y., and Kuipers, O.P. (2013) Zirex: a novel zinc-regulated expression system for *Lactococcus lactis*. *App Environ Microbiol* **79**: 4503–4508.
- Mura, A., Fadda, D., Perez, A.J., Danforth, M.L., Musu, D., Rico, A.I., et al. (2017) Roles of the essential protein FtsA in cell growth and division in *Streptococcus pneumoniae*. *J Bacteriol* **199**: e00608-16.
- Ng, W.L., Tsui, H.C., and Winkler, M.E. (2005) Regulation of the *pspA* virulence factor and essential *pcsB* murein biosynthetic genes by the phosphorylated VicR (YycF) response regulator in *Streptococcus pneumoniae*. *J Bacteriol* **187**: 7444–7459.

- Nicastro, G., Taylor, I.A., and Ramos, A. (2015) KH-RNA interactions: back in the groove. *Curr Opin Struct Biol* **30**: 63–70.
- Oliver, M.B., and Swords, W.E. (2015) Pneumococcal biofilms and bacterial persistence during otitis media. In: *Streptococcus pneumoniae Molecular Mechanisms of Host-Pathogen Interactions*. Brown, J., Hammerschmidt, S., and Orihuela, C.J. (eds). London, UK: Academic Press, pp. 293–308.
- van Opijnen, T., and Camilli, A. (2012) A fine scale phenotype-genotype virulence map of a bacterial pathogen. *Genome Res* **22**: 2541–2551.
- Ortiz, C., Natale, P., Cueto, L., and Vicente, M. (2016) The keepers of the ring: regulators of FtsZ assembly. *FEMS Microbiol Rev* **40**: 57–67.
- Pazos, M., Peters, K., and Vollmer, W. (2017) Robust peptidoglycan growth by dynamic and variable multi-protein complexes. *Curr Opin Microbiol* **36**: 55–61.
- Philippe, J., Vernet, T., and Zapun, A. (2014) The elongation of ovococci. *Microb Drug Resis* **20**: 215–221.
- Pinho, M.G., Kjos, M., and Veening, J.W. (2013) How to get (a)round: mechanisms controlling growth and division of coccoid bacteria. *Nat Rev Microbiol* **11**: 601–614.
- Ramos-Montañez, S., Tsui, H.C., Wayne, K.J., Morris, J.L., Peters, L.E., Zhang, F., *et al.* (2008) Polymorphism and regulation of the *spxB* (pyruvate oxidase) virulence factor gene by a CBS-HotDog domain protein (SpxR) in serotype 2 *Streptococcus pneumoniae*. *Mol Microbiol* **67**: 729–746.
- Rismondo, J., Cleverley, R.M., Lane, H.V., Grosshennig, S., Steglich, A., Moller, L., *et al.* (2016) Structure of the bacterial cell division determinant GpsB and its interaction with penicillin-binding proteins. *Mol Microbiol* **99**: 978–998.
- Rochat, T., Boulouc, P., Yang, Q., Bossi, L., and Figueroa-Bossi, N. (2012) Lack of interchangeability of Hfq-like proteins. *Biochimie* **94**: 1554–1559.
- Rochat, T., Delumeau, O., Figueroa-Bossi, N., Noirot, P., Bossi, L., Dervyn, E., and Boulouc, P. (2015) Tracking the elusive function of *Bacillus subtilis* Hfq. *PLoS One* **10**: e0124977.
- Rued, B.E., Zheng, J.J., Mura, A., Tsui, H.T., Boersma, M.J., Mazny, J.L., *et al.* (2017) Suppression and synthetic-lethal genetic relationships of Δ *gpsB* mutations indicate that GpsB mediates protein phosphorylation and penicillin-binding protein interactions in *Streptococcus pneumoniae* D39. *Mol Microbiol* **103**: 931–957.
- Ruiz, N. (2015) Lipid Flippases for bacterial peptidoglycan biosynthesis. *Lipid Insights* **8**: 21–31.
- Saadeh, B., Caswell, C.C., Chao, Y., Berta, P., Wattam, A.R., Roop, R.M., II, and O'Callaghan, D. (2015) Transcriptome-wide identification of Hfq-associated RNAs in *Brucella suis* by deep sequencing. *J Bacteriol* **198**: 427–435.
- Sauerbier, J. (2012) Horizontaler Gentransfer zwischen *Streptococcus mitis* und *Streptococcus pneumoniae* – Analyse der Resistenzentwicklung. In *Fachbereich Biologie*. Technische Universität Kaiserslautern.
- Sham, L.T., Barendt, S.M., Kopecky, K.E., and Winkler, M.E. (2011) Essential PcsB putative peptidoglycan hydrolase interacts with the essential FtsXSpn cell division protein in *Streptococcus pneumoniae* D39. *Proc Natl Acad Sci USA* **108**: E1061–E1069.
- Sham, L.T., Tsui, H.C., Land, A.D., Barendt, S.M., and Winkler, M.E. (2012) Recent advances in pneumococcal peptidoglycan biosynthesis suggest new vaccine and antimicrobial targets. *Curr Opin Microbiol* **15**: 194–203.
- Shiomi, D., Toyoda, A., Aizu, T., Ejima, F., Fujiyama, A., Shini, T., *et al.* (2013) Mutations in cell elongation genes *mreB*, *mrdA* and *mrdB* suppress the shape defect of RodZ-deficient cells. *Mol Microbiol* **87**: 1029–1044.
- Siegel, S.J., and Weiser, J.N. (2015) Mechanisms of Bacterial colonization of the respiratory tract. *Annu Rev Microbiol* **69**: 425–444.
- Skinner, M.E., Uzilov, A.V., Stein, L.D., Mungall, C.J., and Holmes, I.H. (2009) JBrowse: a next-generation genome browser. *Genome Res* **19**: 1630–1638.
- Stamsås, G.A., Straume, D., Ruud Winther, A., Kjos, M., Frantzen, C.A., and Håvarstein, L.S. (2017) Identification of EloR (Spr1851) as a regulator of cell elongation in *Streptococcus pneumoniae*. *Mol Microbiol* **105**: 954–967.
- Straume, D., Stamsås, G.A., Berg, K.H., Salehian, Z., and Håvarstein, L.S. (2017) Identification of pneumococcal proteins that are functionally linked to penicillin-binding protein 2b (PBP2b). *Mol Microbiol* **103**: 99–116.
- Sung, C.K., Li, H., Claverys, J.P., and Morrison, D.A. (2001) An rpsL cassette, Janus, for gene replacement through negative selection in *Streptococcus pneumoniae*. *Appl Environ Microbiol* **67**: 5190–5196.
- Tsui, H.C., Mukherjee, D., Ray, V.A., Sham, L.T., Feig, A.L., and Winkler, M.E. (2010) Identification and characterization of noncoding small RNAs in *Streptococcus pneumoniae* serotype 2 strain D39. *J Bacteriol* **192**: 264–279.
- Tsui, H.C., Boersma, M.J., Vella, S.A., Kocaoglu, O., Kuru, E., Peceny, J.K., *et al.* (2014) Pbp2x localizes separately from Pbp2b and other peptidoglycan synthesis proteins during later stages of cell division of *Streptococcus pneumoniae* D39. *Mol Microbiol* **94**: 21–40.
- Tsui, H.C., Zheng, J.J., Magallon, A.N., Ryan, J.D., Yunck, R., Rued, B.E., *et al.* (2016) Suppression of a deletion mutation in the gene encoding essential PBP2b reveals a new lytic transglycosylase involved in peripheral peptidoglycan synthesis in *Streptococcus pneumoniae* D39. *Mol Microbiol* **100**: 1039–1065.
- Turner, R.D., Vollmer, W., and Foster, S.J. (2014) Different walls for rods and balls: the diversity of peptidoglycan. *Mol Microbiol* **91**: 862–874.
- Typas, A., Banzhaf, M., Gross, C.A., and Vollmer, W. (2012) From the regulation of peptidoglycan synthesis to bacterial growth and morphology. *Nat Rev Microbiol* **10**: 123–136.
- Ulrych, A., Holečková, N., Goldová, J., Doubravová, L., Benada, O., Kofroňová, O., *et al.* (2016) Characterization of pneumococcal Ser/Thr protein phosphatase phpP mutant and identification of a novel PhpP substrate, putative RNA binding protein Jag. *BMC Microbiol* **16**: 247.
- Updegrave, T.B., Zhang, A., and Storz, G. (2016) Hfq: the flexible RNA matchmaker. *Curr Opin Microbiol* **30**: 133–138.
- Valverde, R., Edwards, L., and Regan, L. (2008) Structure and function of KH domains. *FEBS J* **275**: 2712–2726.

- Van Assche, E., Van Puyvelde, S., Vanderleyden, J., and Steenackers, H.P. (2015) RNA-binding proteins involved in post-transcriptional regulation in bacteria. *Front Microbiol* **6**: 141.
- Vernatter, J., and Pirofski, L.A. (2013) Current concepts in host-microbe interaction leading to pneumococcal pneumonia. *Curr Opin Infect Dis* **26**: 277–283.
- Vinella, D., Joseleau-Petit, D., Thevenet, D., Bouloc, P., and D'Ari, R. (1993) Penicillin-binding protein 2 inactivation in *Escherichia coli* results in cell division inhibition, which is relieved by FtsZ overexpression. *J Bacteriol* **175**: 6704–6710.
- Vollmer, W., Joris, B., Charlier, P., and Foster, S. (2008) Bacterial peptidoglycan (murein) hydrolases. *FEMS Microbiol Rev* **32**: 259–286.
- Walsh, C., and Wencewicz, T. (2016) *Antibiotics: Challenges, Mechanisms, Opportunities*. Washington, DC: ASM Press.
- Wayne, K.J., Sham, L.T., Tsui, H.C., Gutu, A.D., Barendt, S.M., Keen, S.K., and Winkler, M.E. (2010) Localization and cellular amounts of the WalRKJ (VicRKX) two-component regulatory system proteins in serotype 2 *Streptococcus pneumoniae*. *J Bacteriol* **192**: 4388–4394.
- Westesson, O., Skinner, M., and Holmes, I. (2013) Visualizing next-generation sequencing data with JBrowse. *Brief Bioinform* **14**: 172–177.
- WHO. (2017) *List of Bacteria for Which New Antibiotics Are Urgently Needed*. Geneva, Switzerland: World Health Organization. [WWW document]. URL <http://www.who.int/mediacentre/news/releases/2017/bacteria-antibiotics-needed/en/>
- Zapun, A., Vernet, T., and Pinho, M.G. (2008) The different shapes of cocci. *FEMS Microbiol Rev* **32**: 345–360.
- Zheng, J.J., Sinha, D., Wayne, K.J., and Winkler, M.E. (2016) Physiological roles of the dual phosphate transporter systems in low and high Phosphate conditions and in capsule maintenance of *Streptococcus pneumoniae* D39. *Front Cell Infect Microbiol* **6**: 63.

Supporting information

Additional supporting information may be found in the online version of this article at the publisher's web-site.